Transformative 3d-4f coordination clusters carriers

Article (Accepted Version)

Transformative 3d-4f Coordination Clusters Carriers

Kieran Griffiths, George E. Kostakis*

Department of Chemistry, School of Life Sciences, University of Sussex, Brighton BN1 9QJ, UK. E-mail: G.Kostakis@sussex.ac.uk

Abstract

The aim of this perspective is to summarise the use of the reported 3d-4f Coordination Clusters (CCs) in catalytic reactions and to demonstrate the potential of this emerging field. The pioneering work of Shibasaki, Matsunaga and others, demonstrated the use of 3d-4f *in situ* systems to catalyse asymmetric organic transformations. Our recent studies show that well characterised 3d-4f CCs catalyse numerous organic transformations and useful mechanistic aspects of their catalysis can be obtained. Furthermore, we have shown that by manipulation of the metal ion coordination environment; the nature of the 3d and lanthanide ions and the organic periphery of the ligand can all improve the efficacy of a 3d-4f CC catalyst. All *in-situ* formed and well characterized 3d-4f CCs involved in catalysis are discussed.

Contents

1.0 Introduction

Coordination clusters (CCs), formed from organic ligands, transition metal (3d) ions and/ or lanthanide (4f) ions constitute a large class of materials prized for their wide range of properties.[1–7] Traditionally, syntheses of 3d-4f CCs relied upon "serendipitous assembly" resulting in the preparation of CCs which could not be rationally predicted. This method has resulted in high nuclearity CCs[8,9] and molecules with a wide range of interesting properties including luminescence,[10–13] significant magneto-caloric effects (MCEs)[14–16] and single molecule magnetic (SMM) behaviour.[17–19] SMM behaviour has led to the main applications of 3d-4f CCs, with many developments resulting from the study of 3d-4f paradigms which include $Cu^{II}_2Tb^{III}_2$,[20] $Mn^{II}_{18}Dy^{III}$ [21] and $Co^{II}_2Dy^{III}_2$.[22] However since fine control over the coordination environment around 4f ions in mononuclear complexes, which maximises the axial field (for oblate Dy^{III} ions) and therefore gives extremely large U_{eff} and T_B values for the resultant SMM,[23,24] the usefulness of 3d-4f CCs as SMM materials is stunted until similar synthetic control can be developed for 3d-4f CCs. The recent report of a ring-shaped $Fe^{III}_{10}Gd^{III}_{10}$ CC that tops the spin record for a single molecule may bring a new impetus in the field of molecular magnetism,[1] but until these pathways can be completely understood, there are many under-exploited avenues for 3d-4f CCs which can be explored.

One of the most interesting applications of coordination compounds, catalysis, is far less studied for 3d-4f heterometallic CCs with classical N- or O-donor ligands than for organometallic compounds. This difference may be attributed to the mainly low nuclearity of organometallic compounds, which enables possible mechanisms to be determined easily. However, the advantages of using 3d-4f CCs as catalysts becomes evident when the sheer variety of ligand types[25] and the number of 3d and 4f elements are considered.

Synthetic wise, in 3d-4f CCs, 3d or 4f metal ions can be targeted and selectively substituted either by 3d or 4f ions with similar coordination properties, often without altering the topology of the core. This has been reported for numerous 4f-4f ion and 3d-3d ion substitutions.[26–30] With both 3d and 4f elements present in a single molecule, some interesting advantages in both catalytic behaviour and in the study of the reaction mechanisms can be derived. For example, all Ln^{III} (Ln = La, Ce, Pr, Nd, Sm, Eu, Gd, Tb, Dy, Ho, Er, Tm, Yb and Lu) analogues can be synthesised and screened, with little adaptation of the synthetic procedure, due to their similar coordination behaviour. Moreover, in this category Y^{III} can be included because it has a size and Lewis acidity similar to Ho^{III}, and diamagnetic character that allows a catalytic reaction to be monitored with NMR (^1H, ^{13}C, ^{15}N or ^{89}Y). With a more careful and rationalised approach it may also be possible to exchange 3d ions in the same oxidation

state (Co^{II}, Ni^{II}, Cu^{II}, Zn^{II}, Mn^{II}, Fe^{II} and Mn^{III}, Fe^{III}, Co^{III}, Cr^{III}) without distorting the core topology and some of these ions could show unique catalytic properties.

The same approach could enable various techniques to be applied to study the stability of the catalyst and mechanistic aspects. For example, with a catalytically active $Zn^{II}Dy^{III}$ CC it would be very difficult to interpret substrate interactions by ^{1}H NMR or ^{13}C NMR due to the paramagnetic Dy^{III} ($^{6}H_{15/2}$) ions. However, an isostructural $Zn^{II}Y^{III}$ CC would be fully diamagnetic. Furthermore, ^{89}Y NMR could give further insight.[31] In a similar fashion, Dy^{III} may be replaced with Gd^{III} ($^{8}S_{7/2}$ ground state) so that electron paramagnetic resonance (EPR) can be used to identify changes in coordination environment within the CC.[32,33]

In terms of catalytic usefulness, the 4f centres retain their catalytic activity in the presence of Lewis basic N groups allowing their use with unprotected amines,[34] whereas the 3d centres can be redox active.[35,36] Previous studies had concentrated on development of *in situ* 3d/4f/ligand reaction systems to promote asymmetric transformations. The first 3d-4f CC catalyst was reported by Shibasaki, who had described a wide range of homo and heterobimetallic dinuclear CCs which are postulated to form *in situ* and promote a variety of co-operative asymmetric transformations. These dinuclear CCs are supported Schiff base ligands based on the chiral dinucleating ligands reported by Kozlowski *et al*, (Chart 1, H_2**L1** and H_2**L2**) which mononuclear complexes promote the asymmetric conjugate addition of dibenzyl malonate to cyclic enones,[37–39] and the asymmetric ring opening of meso-epoxides with thiols and selenols.[40,41]

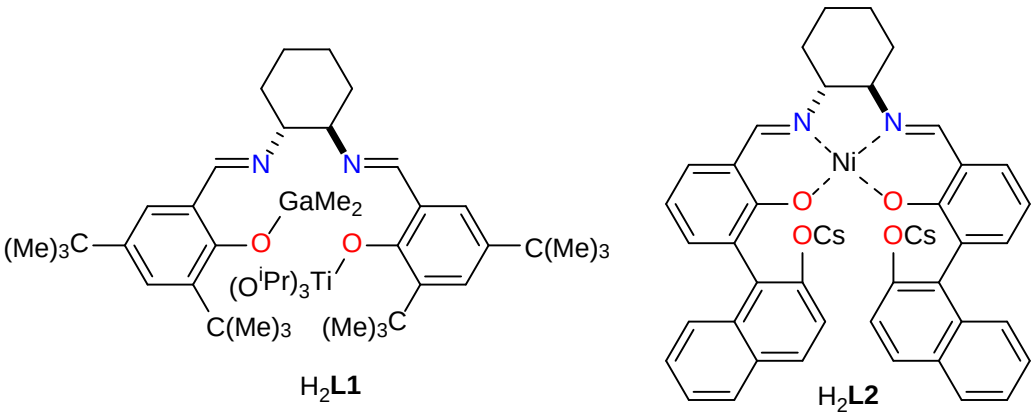

Chart 1. Schiff base ligand complexes reported by Kozlowski *et al* for asymmetric transformations.

These Schiff base ligands share a common ligand structure (Scheme 1) and contain two specific cavities for coordinating metal ions. The first is the N_2O_2 cavity which preferentially coordinates transition metal ions, the second the O_2O_2 cavity which can selectively coordinate

oxophilic lanthanide ions. This specificity is important as all the reported protocols involve the formation of the active species during reaction and the CC catalysts and have not been characterised independently. The geometry of ligand frame brings the two metal ions into proximity (3.5 – 6 Å) which is essential for promoting co-operative catalysis.[42,43]

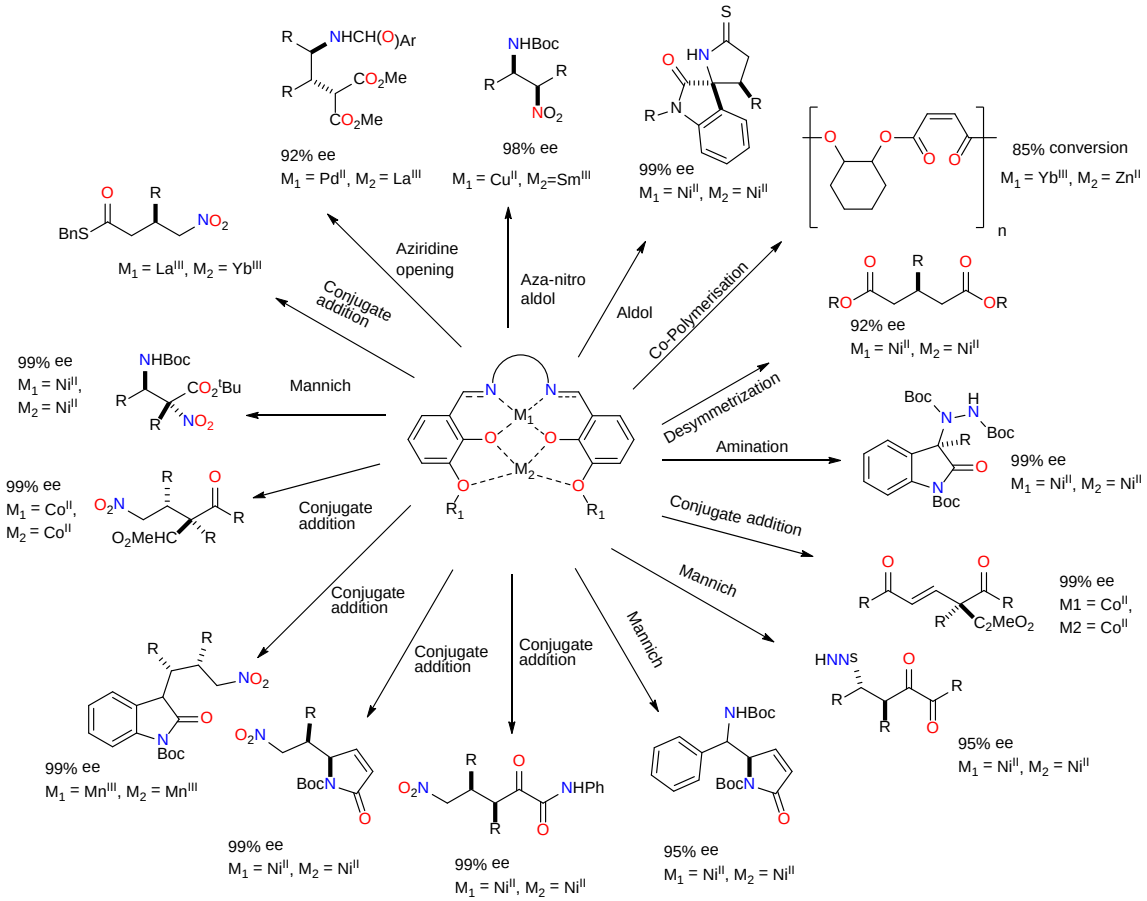

Scheme 1. Heterometallic and homometallic CCs supported by Schiff base ligands for asymmetric transformations.

Various homometallic dinuclear CCs supported by these ligands have been reported to form *in situ* and to promote a variety of asymmetric catalytic transformations (Scheme 1). A bimetallic Ni^{II}_2 catalyst, bearing a 1,1 binaphthyldiamine as a chiral diamine, was particularly versatile and promoted Mannich,[44–46] conjugate addition,[47–49] amination,[50] desymmetization[51] and aldol type reactions.[52,53] By substituting Ni^{II} ions and the chiral diamine linker, it was possible to limit the catalytic efficacy of this system to specific reactions with Co^{II} and Mn^{III} analogues giving 1,4 additions.[54–56] Though bimetallic species are postulated to form, few of these have been characterised, with most examples involving an *in situ* catalytic protocol and only a few examples include Electrospray Ionization Mass Spectrometry studies (ESI-MS) of the catalytic solution.[57,58] The first example of a 3d-4f CC was a dinuclear $Cu^{II}Sm^{III}$ CC, supported by a

Schiff base ligand (Scheme 1), which promoted a *syn*-selective asymmetric nitro-Mannich reaction.[58] Enantioselectivity was further enhanced by replacing the $Cu^{II}Sm^{III}$ core a with $Pd^{II}La^{III}$ core, which permitted the use of aldehydes as electrophiles leading to an *anti-syn* selective nitro aldol reaction.[59,60] The $Cu^{II}Sm^{III}$ CC will be described in the following section.

2.0 3d-4f CC as catalysts

2.1 *in situ* synthesised 3d-4f catalysts for asymmetric transformations

The first 3d-4f CCs used for catalysis were postulated to form *in situ* and use the Schiff base ligands shown in Chart 2, (H_2**L3** – H_2**L6**) which are built from chiral diamines to promote selectivity. These have been successfully employed for one-pot asymmetric transformations and require no previous synthesis of the catalyst. Catalytic substrates, 3d metal salt, 4f metal salt, additive and ligand are mixed in a solvent and left until the catalytic transformation is complete. The ligands share similar structural features, with well-defined pockets for coordination of 3d or 4f ions and hold the metal ions in proximity.

The first and most well studied example of a 3d-4f CC as a co-operative catalyst was for a *syn*-selective asymmetric nitro-Mannich reaction.[57,58] In the first report, a bimetallic Lewis acid/Brønsted base $Cu^{II}Sm^{III}$ CC (**1-CuSm**) was postulated to form *in situ* from the combination of $Cu(OAc)_2$, $Sm(O\text{-}iPr)_3$ (HO-iPr is isopropanol), H_2**L3** and an achiral phenol additive. The optimal system catalysed various aromatic, heteroaromatic, and aliphatic, N-protected, N-Boc imines, giving products in 83-99% *ee* with *syn*/*anti* = >20:1-13:1.[58] (Scheme 2). It was suggested that the dinucleating Schiff base, H_2**L3**, supports the CC with the Cu^{II} ion coordinated to the N_2O_2 cavity and the Sm^{III} ion in the O_2O_2 pocket to give the Cu^{II}-Sm^{III} species.

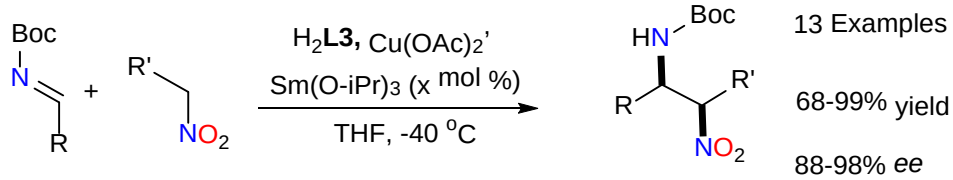

Scheme 2. The $Cu^{II}/Sm^{III}/H_2$**L3** catalysed nitro-Mannich reaction.

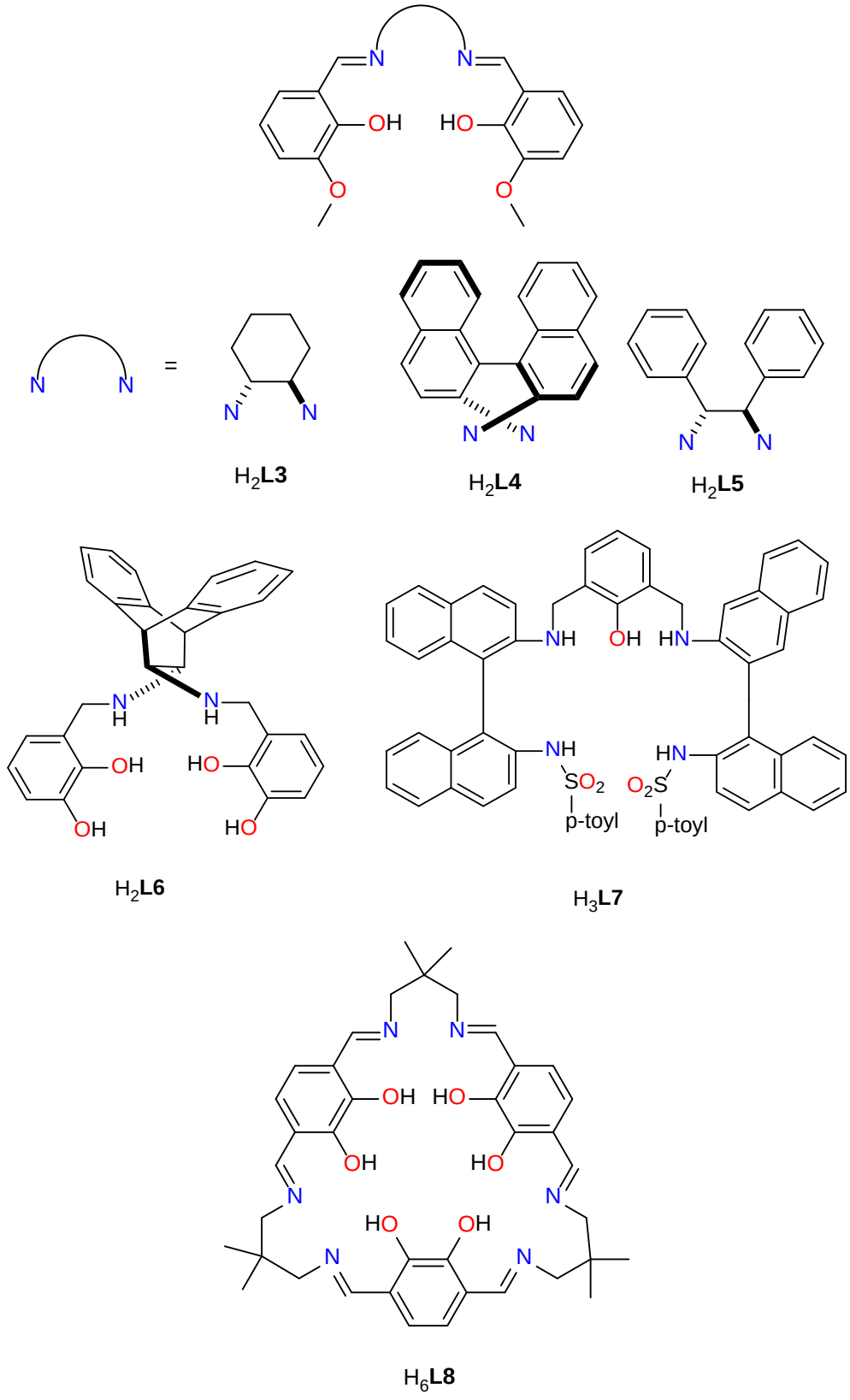

Chart 2. Schiff base and Schiff base-derived ligands used for 3d-4f *in situ* co-operative catalysis.

In the initial investigative steps, with the use of other M^{II} ions (Zn^{II} and Ni^{II}) no conversion to product was observed (Table 1, entries 10 and 11), possibly due to the formation of the tri-and tetra-metallic species which are well known in the literature with ligands like H_2**L3**.[61–65] Replacement of the Sm^{III} salt by other Ln^{III} salts resulted in lower yields (63 -96 %) with reduced stereroselectivity (3:1 > 20:1) and enantioselectivity (5 - 80 %) (Table 1, entries 1 - 9). The effectiveness of the Cu^{II}-Ln^{III} catalysts roughly follows the Lewis acidity of the Ln^{III} series; complexes with the most Lewis acidic (Sm^{III}, Eu^{III} and Gd^{III}) lanthanides give the best performance and complexes with earlier lanthanides a worse performance.

Table 1. Optimisation Studies for the nitro-Mannich reaction catalysed by $M^{II}Ln^{III}$ *in situ* catalysts.

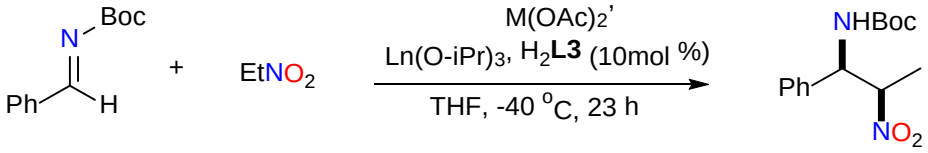

Entries	M^{II} source	Ln^{III} source	M^{II}/Ln^{III}/**L3** ratio	Additive	Yield/ %	dr (*syn*/*anti*)	% *ee* (*syn*)
1	Cu(II)	La	1:1:1	None	73	3:1	5
2	Cu(II)	Pr	1:1:1	None	82	1:1	9
3	Cu(II)	Nd	1:1:1	None	71	>20:1	58
4	Cu(II)	Sm	1:1:1	None	96	>20:1	80
5	Cu(II)	Eu	1:1:1	None	93	>20:1	64
6	Cu(II)	Gd	1:1:1	None	84	13:1	25
7	Cu(II)	Dy	1:1:1	None	89	7:1	48
8	Cu(II)	Er	1:1:1	None	71	11:1	36
9	Cu(II)	Yb	1:1:1	None	63	4:1	6
10	Zn(II)	Sm	1:1:1	None	0		
11	Ni(II)	Sm	1:1:1	None	0		
12	Cu(II)	Sm	1:0.5:1	None	90	16:1	3
13	Cu(II)	Sm	1:2:1	None	81	7:1	3
14	Cu(II)	Sm	1:1:1	4-*tert*-butylphenol	96	>20:1	94

$Cu(OAc)_2$ and $Sm(O\text{-}iPr)_3$ in a 1:1:1 ratio with the ligand were shown to be essential for good reactivity and selectivity (Table 1, entry 4) with changes to the ratio between reactants slightly reducing efficacy and greatly reducing selectivity (Table 1, entries 12 and 13). This again may be explained by the formation of by-products or high order oligomers.[61–65] The co-operative activation of the Sm-Oar moiety as a Brønsted base and Cu^{II} as a Lewis acid was thought to be

the key to the efficacy of this transformation. The scope of the optimised reaction conditions, with a 4-*tert*-butylphenol additive which maximised enantioselectivity, was tested on a limited variety of N-Boc imines and nitroalkanes which all displayed good yields (77-96%) and a high degree of enantioselectivity (83-99%).

The fully study of the Cu^{II}/Sm^{III}/**L3** system introduced a second generation of these catalysts[57] and a plausible catalytic cycle was proposed. ESI-MS studies were used to determine the structure of the CC in solution. Though a trimer of Cu^{II}-Sm^{III} dinuclear CCs was postulated to be the active species, many other oligomers including Cu_1Na_1, Cu_3Sm_3, Cu_6Sm_6, Cu_7Sm_7, Cu_8Sm_8 and Cu_9Sm_9 species were detected by ESI-MS in the Cu: Sm: **L3** system. With addition of the 4-*tert*-butylphenol, the variety of oligomers was reduced to Cu_1Sm_1, Cu_3Sm_3 and/or Cu_6Sm_6 oligomers. However, this still leaves ambiguity in the active species present for the catalysis.

These studies, in conjunction with optical purity studies, which excluded the possibility of a reservoir model, suggested that in the absence of an achiral phenol the oligomeric [$Cu^{II}Sm^{III}$**L3**] species (Cu_1Na_1, Cu_3Sm_3, Cu_6Sm_6, Cu_7Sm_7, Cu_8Sm_8 and Cu_9Sm_9) competitively promoted a Mannich type reaction, resulting in a lower 80% *ee*. Whereas, in the presence of 4-*tert*-butylphenol, 4-*tert*-butylphenol would act as a ligand to Sm, and higher order oligomer species, which were less enantioselective, partially dissociated to form more enantioselective μ-oxo-μ-aryloxy trimer or hexamer as major species. Therefore, the enantioselectivity of the reaction improved to 94 % *ee*. Further kinetic and kinetic isotope effect studies implied that the rate-determining step was the deprotonation of nitroalkane. This data, combined with essential co-operative effect of Cu^{II} and Sm^{III} as confirmed in Table 1, suggested that the co-operative dual activation of nitroalkanes and imines with Cu^{II} and Sm^{III} was important to realize the *syn*-selective catalytic asymmetric nitro-Mannich type reaction.

After these results the catalyst preparation was re-optimised. A second-generation catalytic system from $Sm_5O(OiPr)_{13}$ showed broader substrate generality as well as higher reactivity and stereoselectivity compared to that from $Sm(O\text{-}iPr)_3$ (Scheme 3). The optimal system with $Sm_5O(O\text{-}iPr)_{13}$ could be used with various aromatic, heteroaromatic, and isomerizable aliphatic N-Boc imines, to give products in 66 – 99 % *ee* and *syn*/*anti*) >20:1-13:1.

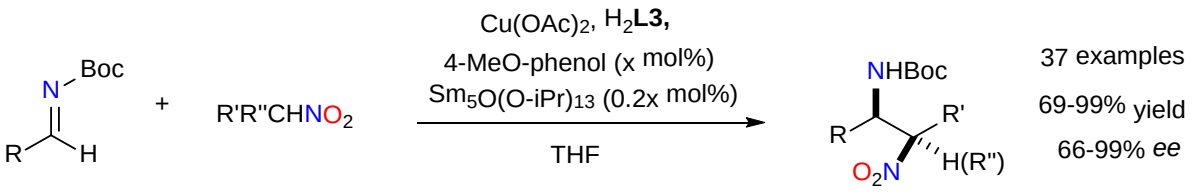

Scheme 3. Second generation of the **1-CuSm** catalyst.

Other more recent studies with *in situ* 3d-4f asymmetric catalysis are less robust and offer little in the way of active species identification or mechanistic insight.[66,67] Zhou *et al.* reported a dinuclear Cu^{II}-Sm^{III} CC (**2-CuSm**) supported by the sulphonamide ligand H_3**L7** which catalysed an *in situ anti*-selective asymmetric Henry reaction between various aldehydes and nitrostyrenes (Scheme 4).[66] *anti*-β-nitro alcohols are obtained in up to 99% conversion >30:1 dr and 98% *ee*. The use of other M^{II} and Ln^{III} ions was not investigated. No conversion was observed when H_3**L7** and $Cu(OAc)_2$ alone was used. In addition, in the reaction with only H_3**L7** and $Sm(OiPr)_3$ the yield was reduced to 90% with 91% *ee*. ESI-MS studies indicated the presence of a [$Cu^{II}Sm^{III}$**L7**] dimer, which was postulated to be the active species, however the monomeric [Cu^{II}**L7**] species is also observed. Though the *in situ* catalysis with H_3**L7** with $Sm(OiPr)_3$ gave a higher yield than the H_3**L7** and Cu(OAc), the species in the more active reaction is not studied via ESI-MS.

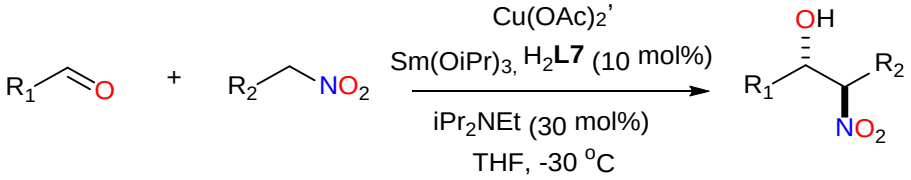

Scheme 4. The $Cu^{II}/Sm^{III}/H_2$**L7** catalysed *anti*-selective asymmetric Henry reaction.[66]

These studies were followed by work on a Ni^{II}-La^{III} CC (**3-NiLa**) based on the dinucleating ligand H_2**L6**. This system catalysed the enantioselective decarboxylation -1,4-addition of malonic acid half thioester to nitroalkenes (Scheme 5).[67] **3-NiLa** gave products in a 40-99% yield and 66-94% *ee*. No further identification or characterisation of the active species was presented.

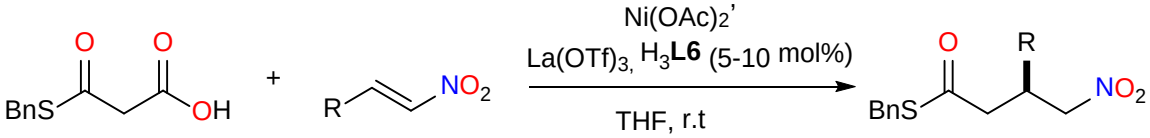

Scheme 5. The $Ni^{II}/La^{III}/H_2$**L6** catalysed asymmetric decarboxylative 1,4-addition of malonic acid half thioester.

2.2 Well characterized 3d-4f based catalysts

The previously described *in situ* 3d-4f CC catalysts have not been synthesised or characterised by X-ray analysis prior to reaction and have been made *in situ*; the catalytic entities are assumed to be dinuclear and are identified only by ESI-MS; the M^{II} and Ln^{III} ions are held within a single dinucleating Schiff base or Schiff base-like framework of low nuclearity. Few attempts have been made to identify a catalytic mechanism and to study the catalyst by techniques such as ^{1}H NMR, EPR, ESI-MS and UV/Vis spectroscopy. With the aim of developing a new generation of 3d-4f CC catalysts, our group developed a series of well-characterised 3d-4f CC pre-catalysts, in which substitution of 3d and 4f ions within the defined framework could lead to enhanced catalytic efficacy and more detailed study of the catalytic cycle.

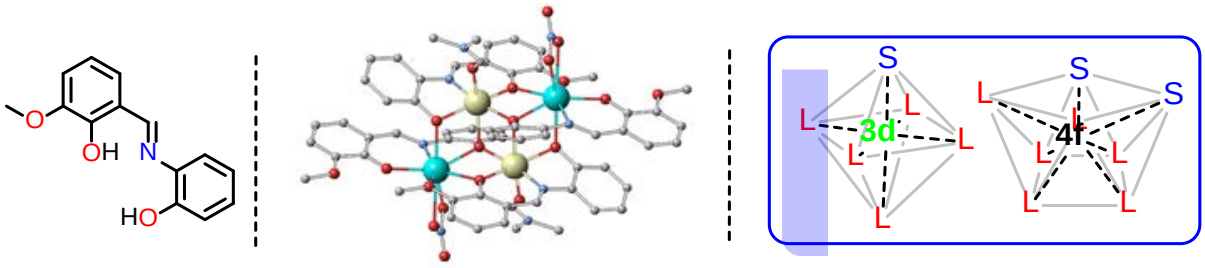

Figure 1. (Left) The organic ligand H_2**L9** used to yield the defect dicubane motif shown in the middle. (right) A representation of the coordination environment of the 3d and 4f ions in this motif

Previously, Powell *et al.* reported a series of tetranuclear defect dicubane (Figure 1) $[M^{II}_2Ln^{III}_2(\mathbf{L9})_4(NO_3)(THF)_2]$ (M = Ni, Co) CCs supported by H_2**L9**, which displayed SMM behaviour.[22,68] Analogues of these CCs with a modified coordination sphere, represented an ideal starting point for developing well-characterized isoskeletal 3d-4f CC catalysts, as it had already been shown that both M^{II} and Ln^{III} centres could be substituted without altering the structure and topology of the molecule. As H_2**L9** is a Schiff base ligand (Figure 1), a wide variety of modified aldehyde and aminophenol precursors may be used to give a range of ligands with the same core topology.

With the aim of altering the coordination environment around the 3d and 4f metal ions and modifying the organic periphery in the previously described defect dicubane molecular structure, a full synthetic study was devised to discover a reliable synthetic route to these molecules.[69] This study highlighted the synthetic problems involved in the crystallisation of the isoskeletal defect dicubane molecules including; oxidation; solubility issues; solvent type;

co-ligand; crystallisation method and metal salt. These results highlight the importance of characterising the 3d-4f CCs if the catalytic system is to be fully understood and throws doubt on to the postulated dinuclear structures in previous work. The CCs were made as usual by adding 3d metal and 4f metal salts to a stirred mixture of solvent and ligand. The solutions are stirred and crystals formed by SE or vapour diffusion (VD). A table of synthetic conditions and general formulae for the catalysts are shown in Table 2. These defect dicubane CCs are isoskeletal and formed in the absence of co-ligands. In this topology, the four metal ions are linked together by two μ_3-O and further bridged by four μ_2-O, forming a $M^{II}_2Ln^{III}_2O_6$ core. The two 3d ions and two 4f ions can be co-planar, and the six oxygen atoms are located above and below the plane with centrosymmetric feature. The Schiff base organic ligands (**LX**) exhibit two different coordination modes (Figure 2). In the first mode (Figure 2, mode I), the two phenoxide oxygen atoms and the imine nitrogen atom are chelated to the M^{II} centre, and the two phenoxide atoms are further bonded to two Ln^{III} ions and the methoxide oxygen atoms is bound to Ln^{III}. In the second mode (Figure 2, mode II), the two phenoxide oxygen atoms and the imine nitrogen atom are chelated to the Ln^{III} centre, while the phenoxide oxygen atom (from the 2-aminophenol unit), is further bound to two M^{II} centres. ESI-MS of all compounds display two prominent peaks in the MS (positive-ion mode) which correspond to one dianionic fragment and one anionic fragment. These peaks usually correspond to the general formulas $[M^{II}_2Ln^{III}_2(\mathbf{LX})_4]^{2+}$ and $[M^{II}_2Ln^{III}_2(\mathbf{LX})_4(CA)_x(solv)_y]^{+}$ and indicate that the tetranuclear $[M^{II}_2Ln^{III}_2(\mathbf{LX})_4]^{2+}$ core is stable in the solution.

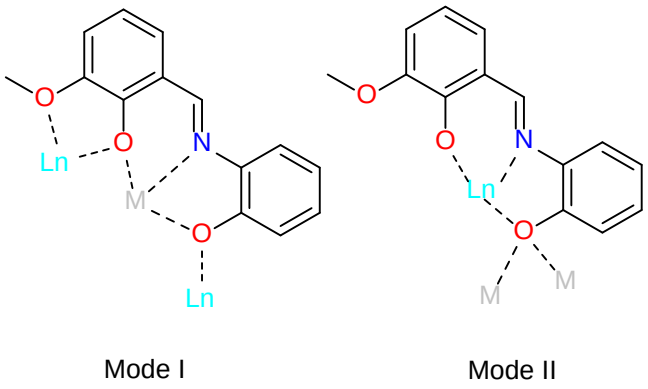

Figure 2. Observed coordination modes in $M^{II}_2Ln^{III}_2$ defect dicubane CCs.

Table 2. Synthetic conditions used to synthesise the reported tetranuclear 3d-4f CC catalysts.

Entry	Formula	Ln^{III} salt	M^{II} salt	Ligand	Solvent	Ratio (Ln:M:**L**:Et_3N)	Crystallization method
1	$[Ni^{II}_2Dy^{III}_2$(**L9**)$_4(EtOH)_6](ClO_4)_2$ (**8-NiDy**)	$Ln(OTf)_3\cdot 5H_2O$	$Ni(ClO)_4\cdot 6H_2O$	H_2**L9**	EtOH	1:1:2:5	SE
2	$[Co^{II}_2Dy^{III}_2$(**L9**)$_4(EtOH)_6](ClO_4)_2$ (**8-CoDy**)	$Ln(OTf)_3\cdot 5H_2O$	$Co(ClO)_4\cdot 6H_2O$	H_2**L9**	EtOH	1:1:2:5	SE
3	$[Ni^{II}_2Dy^{III}_2$(**L9**)$_4Cl_2(MeCN)_2]$ **(9-NiDy)**	$Ln(OTf)_3\cdot 5H_2O$	$Ni(ClO)_4\cdot 6H_2O$	H_2**L9**	MeCN	1:1:2:5	SE
4	$[Ni^{II}_2Ln^{III}_2$(**L9**)$_4Cl_2(MeCN)_2]$ (**9-NiLn**) Ln = Sm, Eu, Tb, Gd, Y	$LnCl_3\cdot 5H_2O$	$NiCl_2\cdot 6H_2O$	H_2**L9**	MeCN	1:1:2:5	DMF/Et_2O VD
5	$[Zn^{II}_2Ln^{III}_2$(**L9**)$_4(NO_3)_2(DMF)_2]$ (**13-ZnLn**)	$Ln(NO_3)_3\cdot 5H_2O$	$Zn(NO_3)_2\cdot 6H_2O$	H_2**L9**	EtOH	1:2:2:4.5	DMF/Et_2O VD
6	$[Cu^{II}_2Ln^{III}_2$(**L9**)$_4(NO_3)_2(MeCN)_2]$ (**13-CuDy**)	$Ln(NO_3)_3\cdot 5H_2O$	$Cu(NO_3)_2\cdot 4H_2O$	H_2**L9**	MeCN	2:1:2:5	SE
7	$[Zn^{II}_2Ln^{III}_2$(**LX**)$_4(NO_3)_2(DMF)_2]$ (**17-ZnY** – **36-ZnY**, Table 17)	$Y(NO_3)_3\cdot 5H_2O$	$Zn(NO_3)_2\cdot 6H_2O$	H_2**LX**	EtOH	1:2:2:4.5	DMF/Et_2O VD

2.2.1. 3d-4f catalysts for polymerisation

Two Zn^{II}-Ln^{III} CCs have been reported for the co-polymerisation of epoxides.[70,71] The synthetic conditions are shown in Table 3. The most popular of these reactions,[72] carbon dioxide- epoxide co-polymerisations, produce polycarbonates which have many industrial applications, however the biggest drawback of this reaction is the fixation of CO_2.[72] Secondly, the co-polymerisation of epoxide with anhydride is less popular, however the availability of structurally diverse anhydrides enables a wider variety of polymeric backbones for the obtained polyesters. Both polymerisation reactions begin when an epoxide is activated by a Lewis acidic metal centre and undergoes a nucleophilic attack by a suitable initiator, followed a ring opening. Therefore, many metal catalysts have been reported for these reactions.[73,74] The examples of mononuclear and dinuclear complexes which catalyse this reaction such as Zn^{II}_2,[75] Mn^{III},[76] Co^{III} [77]and Cr^{III} [78,79] all contain Salen ligands which have a similar structure to H_2**L3** (Chart 2). Importantly, cooperation in dinuclear Cr^{III} and Co^{II} salen complexes enhanced the catalytic activity over that of their corresponding monomeric analogues.[80,81] These factors inspired the groups to combine the Lewis acidity of Zn^{II} and Ln^{III} ions and Schiff base ligands to form 3d-4f CCs to catalyse these types of epoxide co-polymerisations.

A dinuclear CC with the general formula [$Zn^{II}Yb^{III}$(**L3**)(μ_1-OAc)(μ_1-OAc)(μ_2-OAc)(H_2O)] (**4-ZnYb**) (Figure 3) supported by H_2**L3** has been reported for the solvent-free copolymerization of cyclohexene oxide (CHO) and maleic anhydride (MAH) (Scheme 6).[70] The presence of the co-catalyst thiamine pyrophosphate (TPP) or 4-dimethylaminopyridine (DMAP) leads to the formation of polyester and poly (ester-co-ether) respectively. **4-ZnYb** can effectively catalyse the co-polymerisation alone, unlike similar salen-based M^{III} complexes, which may indicate that $[OAc]^-$ initiators are working co-operatively with the active Zn^{II} and Yb^{III} centres. The structure of a **4-ZnYb** was determined by X-ray crystallography and is isoskeletal to the species postulated by Shibasaki in earlier examples (**1-CuLn**). The structure was further verified by ESI-MS and TGA solid state studies. There was some evidence for weak interactions between substrates and CC in the solid state.

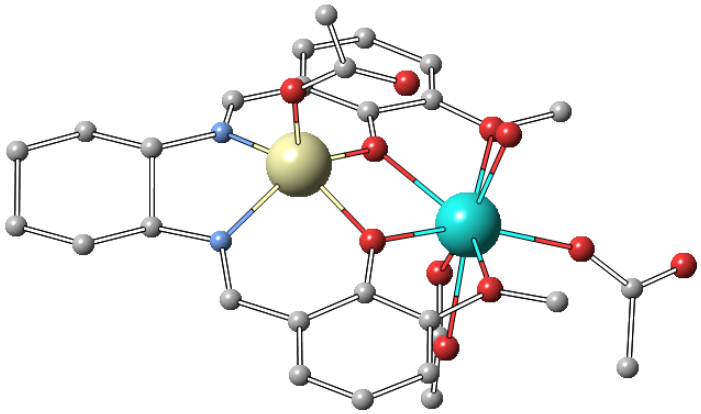

Figure 3. Molecular structure of **4-ZnYb**. Colour code: Yb^{III}, light blue; Zn^{II}, pale yellow; O, red; C, grey and N, pale blue. Hydrogen ions and counter ions are omitted for clarity.

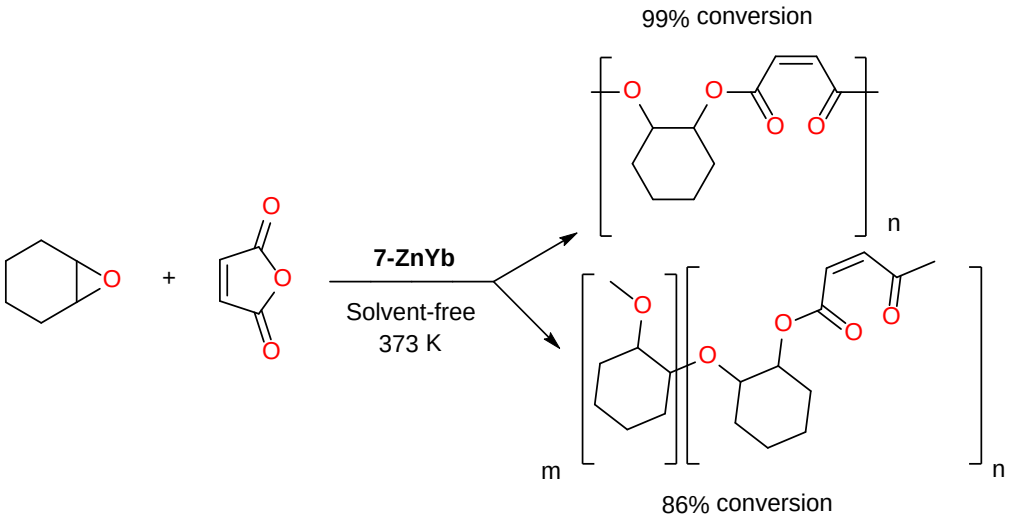

Scheme 6. Solvent free co-polymerisation of CHO and MAH by **4-ZnYb**.

Table 3. Conditions for the synthesis 3d-4f CC polymerisation catalysts.

Entry	General formula	Ln^{III} salt	M^{II} salt	Ligand	Solvent	Ratio (Ln:M:L:B)	Crystallisation method
1	$[Zn^{II}Yb^{III}$(**L3**)$(OAc)_3(H_2O)]$ (**4-ZnYb**)	$Yb(OAc)_3{\cdot}6H_2O$	$Zn(OAc)_2{\cdot}2H_2O$	H_2**L3**	MeOH	1:1:1:0	VD/ Et_2O
2	$[Zn^{II}_3Ln^{III}$(**L8**)$(OAc)_3]$ (**5-ZnLn**) Ln= Ce, Pr, Nd, Sm, Eu, Gd, Dy	$Ln(OAc)_3.xH_2O$	$Zn(OAc)_2{\cdot}2H_2O$	H_6**L8**	MeOH/$CHCl_3$	1:3:3:3	SE
3	$[Zn^{II}_3La^{III}$(**L8**)$(NO_3)_2](NO_3)$ (**6-ZnLa**)	$La(NO_3)_3{\cdot}6H_2O$	$Zn(OAc)_2{\cdot}2H_2O$	H_6**L8**	MeOH/$CHCl_3$	1:3:3:3	SE
4	$[Zn^{II}_3La^{III}$(**L8**)$(OAc)(OTf)_2]$ (**7-ZnLa**)	$La(OTf)_3{\cdot}xH_2O$	$Zn(OAc)_2{\cdot}2H_2O$	H_6**L8**	MeOH/$CHCl_3$	1:3:3:3	SE

A series of tetranuclear 3d-4f CCs, with the general formula $[Zn^{II}_3Ln^{III}$(**L8**)$(OAc)_3]$ (**5-ZnLn**) where Ln = La, Ce, Pr, Nd, Sm, Eu, Gd and Dy, were used to promote the alternating copolymerisation of CHO and CO_2.[71] Initially, a complex with the general formula $[Zn^{II}_3La^{III}$(**L8**)$(OAc)_3]$ (**5-ZnLa**, Figure 4) was synthesised and characterised by X-ray diffraction studies and ^{1}H NMR spectroscopy. Two isoskeletal analogues of **5-ZnLa**, with the general formulas $[Zn^{II}_3La^{III}$(**L8**)$(NO_3)_2]{\cdot}(NO_3)$ (**6-ZnLa**) and $[Zn^{II}_3La^{III}$(**L8**)$(OAc)(OTf)_2]$ (**7-ZnLa**), were synthesised to determine the catalytic effects of different counter ions.

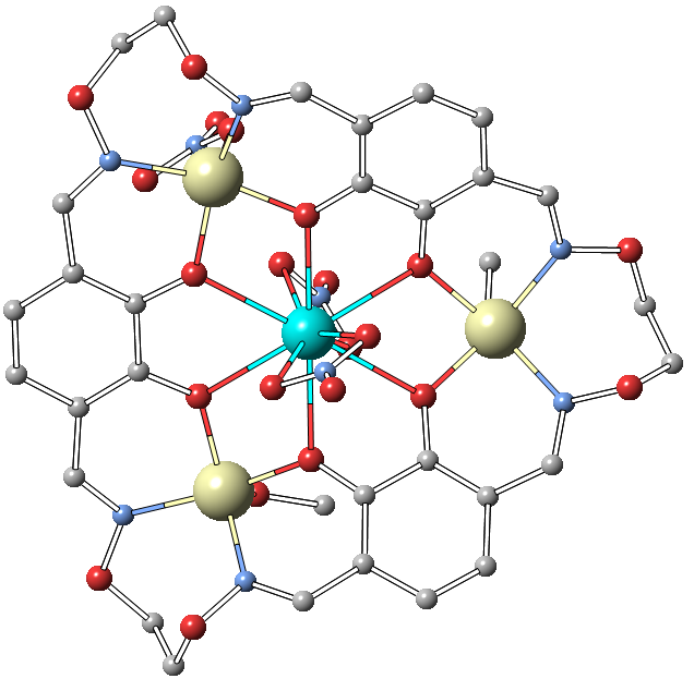

Figure 4. Molecular structure of **5-ZnLa**. Colour code: La^{III}, light blue; Zn^{II}, pale yellow; O, red; C, grey and N, pale blue. Hydrogen ions and counter ions are omitted for clarity.

The three complexes were tested as catalysts for the copolymerisation of CHO and CO_2 which is shown in Table 4, entries 1 - 3. The type of counter-ion was critical for achieving high catalytic yields. **5-ZnLa** was the best catalyst for the copolymerisation in both terms of high activity and almost exclusively carbonate linkages (Table 4, entry 1). Whereas the use of **6-ZnLa** resulted in only trace amounts of the polymer (Table 4, entry 2) and **7-ZnLa** only showed a high catalytic activity for polyether transformation with only 1% carbonate linkage (Table 4, entry 3).

Table 4. Catalytic activity and selectivity of **5-ZnLn**.

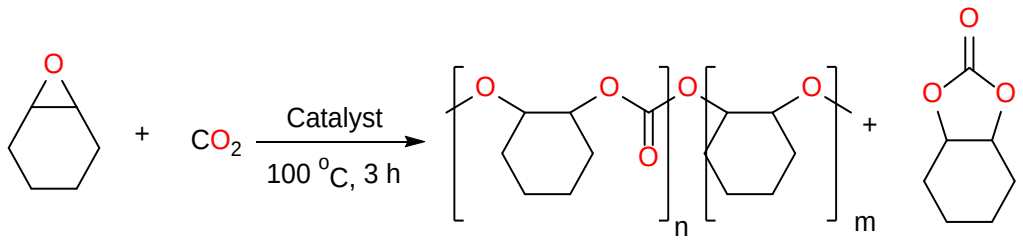

Entry	Catalyst	Lanthanide ion	TOF[a]/ h^{-1}	Carbonate linkages [b]/ %	M_n[c]
1	**5-ZnLa**	La^{III}	230	>99	10000
2	**6-ZnLa**	La^{III}	trace	-	n/a
3	**7-ZnLa**	La^{III}	413	1	n/a
4	**5-ZnCe**	Ce^{III}	370	>99	14,000
5	**5-ZnPr**	Pr^{III}	310	>99	14,000
6	**5-ZnNd**	Nd^{III}	320	>99	18,000
7	**5-ZnSm**	Sm^{III}	290	>99	21,000
8	**5-ZnEu**	Eu^{III}	250	>99	11,000
9	**5-ZnGd**	Gd^{III}	200	>99	11,000
10	**5-ZnDy**	Dy^{III}	100	98	6,600

[a] TOF=mole [CHO] consumed per mole catalyst per hour. [b] Determined by the relative integrals of the ^{1}H NMR resonances at δ=3.45 (polyether) and δ=4.65 ppm (polycarbonate). [c] Determined by GPC in THF, using polystyrene standards as the calibrant

As **5-ZnLa** showed superior catalytic activity, the isoskeletal lanthanide analogues (**5-ZnLn**) were synthesised and tested for the copolymerisation (Table 4, entries 1, 4 - 10). The CCs of

larger lanthanides, such as La, Ce, Pr, and Nd, resulted in higher catalytic activities compared with middle or late lanthanide elements with a very high proportion of carbonate linkages and a narrow molecular weight distribution retained (Table 4, entries 4 – 6). **5-ZnCe** displayed the highest catalytic activity with a high proportion of carbonate linkages and was chosen as the optimal catalyst precursor (Table 4, entry 4). X-ray diffraction studies highlight the different coordination mode of the acetate ions in **5-ZnCe** when compared to **5-ZnLa** and indicates a more rapid fluxionality of the three acetate ligands. Further results show that the addition of excess [^{n}Bu$_4$N][OAc] gradually decreases the weight of the polycarbonate whilst retaining good yields. Moreover, the addition of various ammonium benzoates afforded ArCOO$^-$/HO-terminated polymers with the corresponding benzoate moiety as one terminal group and a hydroxy group as the other terminal group, suggesting that almost all acetate ligands were readily replaced by the added ammonium benzoates. This shows the acetate anions were flexible over not only an intramolecular rapid exchange, but also an intermolecular exchange with outer-sphere ammonium acetates, which resulted in the control of molecular weight as a new type of telomerisation.

2.2.2 Tetranuclear $Ni^{II}_2Ln^{III}_2$ for a ring opening/ electrocyclization reaction.

In 2015,[82] we described two novel tetranuclear defect dicubane shaped CCs with the general formula $[M^{II}_2Dy^{III}_2(\mathbf{L9})_4(solv)_6](ClO_4)_2$, M = Ni (**8-NiDy**), Co (**8-CoDy**). Compounds **8-NiDy** and **8-CoDy** (Figure 5) were isoskeletal to the previously reported $Ni^{II}_2Dy^{III}_2$ and $Co^{II}_2Dy^{III}_2$ SMMs,[22,68] however the coordinated nitrate ions were substituted by solvent EtOH molecules and the charge balanced by perchlorate anions. Solution state studies by ESI-MS showed the presence of monocationic $[M^{II}_2Dy^{III}_2(\mathbf{L9})_4]^+$ or dicationic $[M^{II}_2Dy^{III}_2(\mathbf{L9})_4]^{2+}$ species, indicating the stability of the cores in solution. **8-NiDy** and **8-CoDy** were tested as catalysts for the formation of *trans*-4,5-diaminocyclopent-2-enones from 2-furaldehyde and secondary or primary amines, a transformation catalysed by $Dy(OTf)_3$.[83] This reaction proceeds via the formation of stenhouse salts which result from the furan ring-opening reaction upon condensation of furfurals and amines.[84–86]

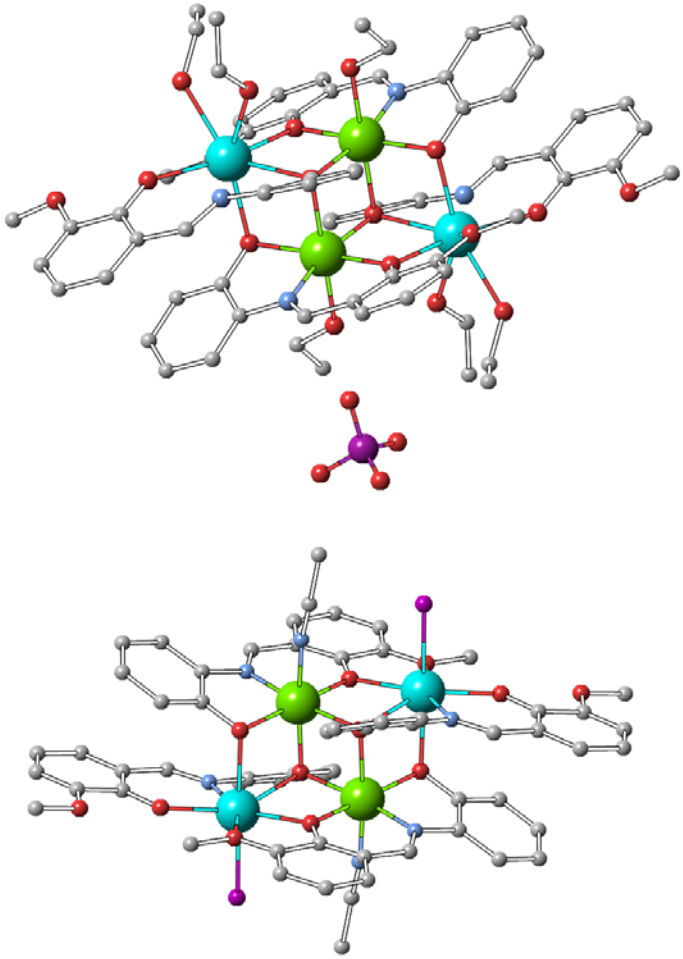

Figure 5. Molecular structures of **8-NiDy** (left) and **9-NiDy** (right). Colour code: Ln^{III}, light blue; Ni^{II}, green; O, red; C, grey; N, pale blue and Cl, purple. Hydrogen ions omitted for clarity.

At room temperature, these CC catalysts performed poorly (Table 5, entries 1-2) however, under reflux the conversion significantly improved (Table 5, entries 4-5). When **8-NiDy** was refluxed in MeCN the isoskeletal $[Ni^{II}_2Dy^{III}_2(\mathbf{L9})_4Cl_2(MeCN)_2]$ (**9-NiDy**) was formed. The incorporation of chloride anions from a perchlorate conversion at the Dy^{III} centres, was confirmed by X-ray analysis (Figure 5). ESI-MS studies confirmed the retention of the $[Ni^{II}_2Ln^{III}_2(\mathbf{L9})_4]^{2+}$ core in solution. When ethanol was substituted for acetonitrile and with a reflux time of 1 h, **9-NiDy** was obtained in good yields. When **9-NiDy** was used for the transformation, conversion drastically improved (Table 5, entry 6), with an order of magnitude reduction in catalyst loading and with mild conditions compared to the previously reported $Dy(OTf)_3$ transformation.[83]

Table 5. Initial catalytic protocols for the 3d-4f catalysed formation of *trans*-4,5-diaminocyclopen-2-enone.

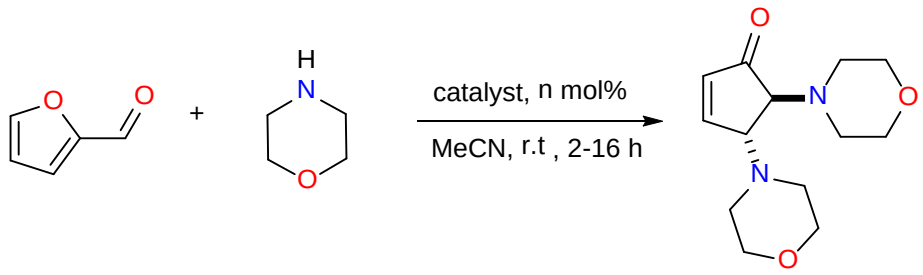

Entries	Catalyst	T	Loading/ mol%	Time / h	Yield/ %
1	$Dy(OTf)_3$	r.t	10	16	quantitative
2	**8-NiDy**	r.t	10	16	55
3	**8-CoDy**	r.t	10	16	41
4	**8-NiDy**	reflux	2.5	2	90
5	**8-CoDy**	reflux	2.5	2	94
6	**9-NiDy**	reflux	1	16	quantitative

The scope of reaction with the optimised reaction conditions and **9-NiDy** was then explored with a variety of secondary amine substrates. With all substrates, the reactions proceeded smoothly and it was possible to isolate the corresponding products in excellent yields (Table 6).

Table 6. The scope of the **9-NiDy** catalysis with secondary amine substrates.

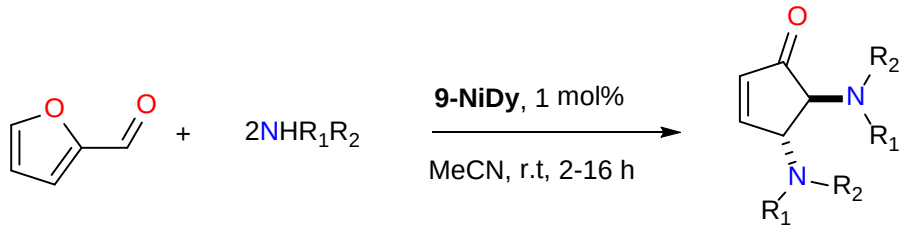

Entries	Substrate	Loading/ %	Yield/ %
1	$O(CH_2CH_2)_2NH$	1	quantitative
2	$(CH_2{=}CHCH_2)_2NH$	1	99
3	C_8H_9N	1	95
4	$C_9H_{11}N$	1	61
5	$C_9H_{11}N$	2.5	99
6	*Iso*-$C_9H_{11}N$	1	63
7	*Iso*-$C_9H_{11}N$	1.5	99

When the same reaction conditions were used with primary amines, **9-NiDy** catalysed the formation of the corresponding Stenhouse salts (Table 7), as has been observed with $Sc(OTf)_3$.[83] The treatment of Stenhouse salt with dilute HCl led to the ring closure of the corresponding *trans*-4,5-diaminocyclopent-2-enones (Scheme 7). These results are consistent with Batey's proposition that the Dy^{III} is not involved in the cyclisation step.[82] DFT studies were presented which also supported this.[82]

Table 7. Scope of **9-NiDy** catalysis with primary amine substrates.

Entries	Substrate	Loading/ %	Yield/ %	Conversion
1	$C_6H_5NH_2$	1	96	99
2	$CH_3OC_6H_4NH_2$	1	62	95
3	$FC_6H_4NH_2$	1	70	n/a
4	$CF_3C_6H_4NH_2$	1	26	n/a

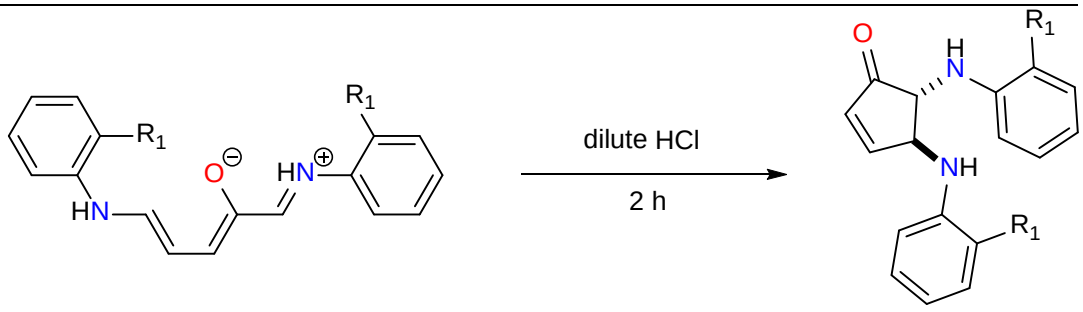

Scheme 7. Acid catalysed ring-closure of a Stenhouse salt.

This report detailed the first examples of a series of custom-designed, catalytically active 3d/Dy^{III} CCs and provided a starting point for the development of heterometallic catalytic CCs. It showed that the catalytic activity could be improved by modifying the coordination of the Dy^{III} ion. It was surmised that substitution of the Dy^{III} ions by Ln^{III} ions would improve the catalytic performance of this type of CC as our next report shows.[87] By applying the synthetic approach previously described for **9-NiDy**, but with various other Ln^{III} salts, led to the isolation of 3d-4f CCs of different core configurations. These were not isoskeletal to the desired structure (Figure 6). These further highlight the importance of the isolation and characterisation of pre-catalytic species in the study of 3d-4f CC catalysis.

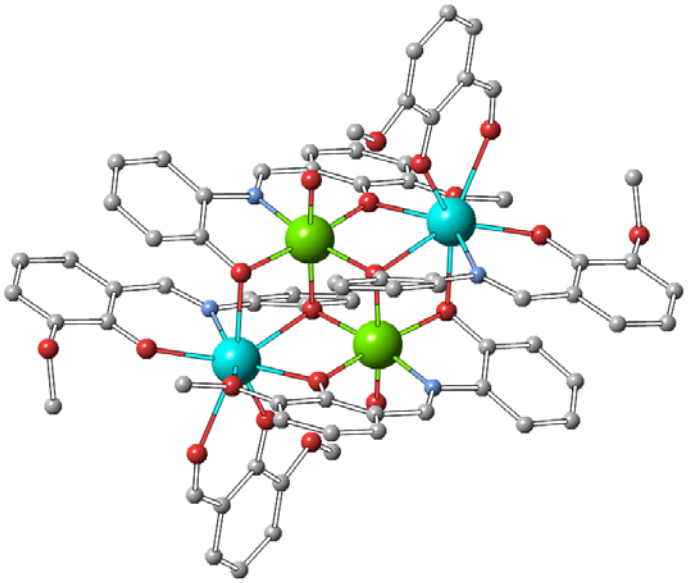

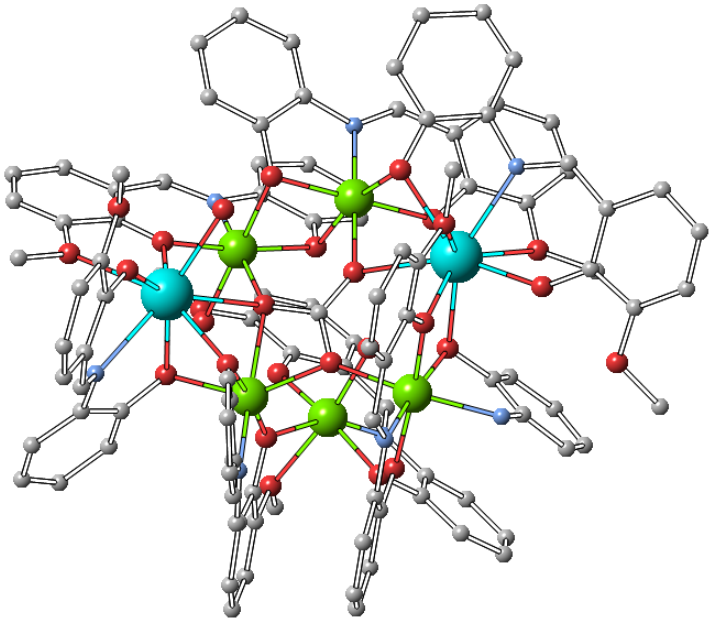

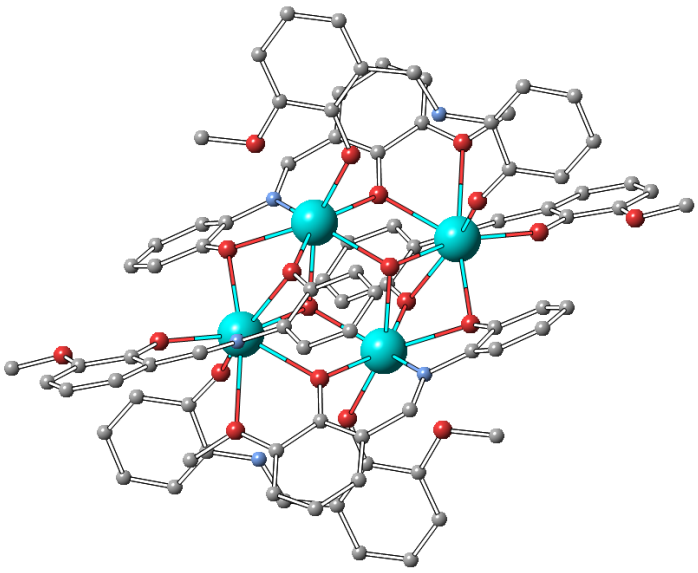

Figure 6. Molecular structures of undesired products from attempted synthesis of **9-NiSm** analogues. $[Ni^{II}_2Sm^{III}_2(\mathbf{L9})_4(o\text{-van})_2(H_2O)_2]\cdot 4CH_3CN$ (upper); $[Ni^{II}_5Sm^{III}_2(CO_3)(\mathbf{L9})_7(\mathbf{L9'})(H_2O)_3]$ (middle) $[Sm^{III}_4(OH)_2(\mathbf{L9})_4(H\mathbf{L9})_2]\cdot 2CH_3CN$ (lower). Colour code-Ln^{III}, light blue; Ni^{II}, green; O, red; C, grey and N, pale blue. Hydrogen ions omitted for clarity.

A large amount of precipitate formed during these reactions and by use of various spectroscopic techniques (TGA, FT-IR, ESI-MS, CHN) it was determined that these were isostructural Ln^{III} (Ln = Sm, Eu, Gd, Tb and Y) analogues of **9-NiDy**. They will be further referred to as **9-NiLn**. The **9-NiLn** series were used as the catalysts for the formation of *trans*-4,5-diaminocyclopent-2-enones from 2-furaldehyde and morpholine, with the optimal conditions reported in the previous publication. Overall, the replacement of the Dy^{III} (Table 8, entry 1) by other Ln^{III} elements led to a decrease in efficacy (Table 8, entries 2 - 5). The increasing yields across the group may be related to the lanthanide contraction. Replacement of Dy^{III} by Y^{III}, which has the same ionic radius, gave the same high yields even with reduced loading (Table 8, entries 6 and 7). Y^{III} analogues have been shown to outcompete Dy^{III} derivatives, but no rationale has been proposed.[88]

Table 8. Comparison of **9-NiLn** CCs catalytic activity.

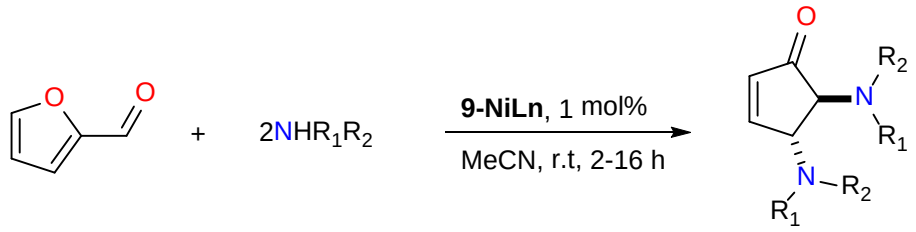

Entries	Catalyst	T	Loading/ mol%	Time/ h	Yield/ %
1	**9-NiDy**	r.t	1	2	quantitative
2	**9-NiSm**	r.t	1	2 (24)	55 (75)
3	**9-NiEu**	r.t	1	2 (24)	60 (99)
4	**9-NiGd**	r.t	1	2 (24)	63 (99)
5	**9-NiTb**	r.t	1	2 (24)	63 (86)
6	**9-NiY**	r.t	1	2	quantitative
7	**9-NiY**	r.t	0.5	2 (24)	98 (100)

In earlier work it had been questioned whether both metal centres had catalytic roles, whether they were co-operative, or whether only one was active. Table 8 confirms that the yield of product was dependent on the substitution of the Ln^{III} ion suggesting it must be involved in the catalytic transformation. Previous results displayed little difference between the efficacy of **8-NiDy** and **8-CoDy** analogues (Table 5, entries 2 and 3). The use of Ni^{II}, Co^{II}, Ln^{III} salts as catalysts demonstrated that a catalyst was necessary for the reaction to progress and that Ni^{II} salts[87] have an almost negligible effect, even up to 30% loading with added ligand, whereas $LnCl_3$ salts without Ni^{II} displayed some conversion to product. Dy^{III} and Y^{III} salts gave the highest yields. These results suggest that only the Ln^{III} node of the **12-NiLn** was catalytically active and that the system was not co-operative.[87]

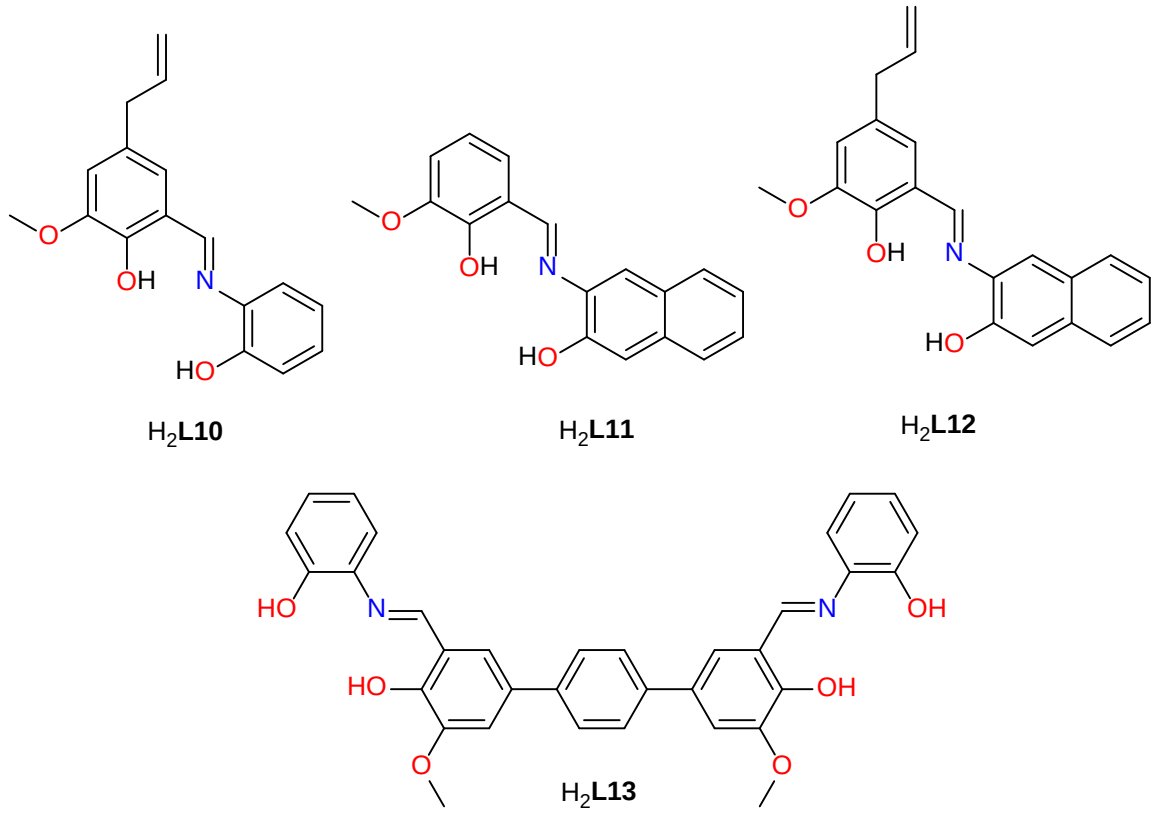

Chart 3. Ligands used for the synthesis of defect-dicubane $Ni^{II}_2Y^{III}_2$ CC catalysts with a modified organic periphery.

Three isoskeletal analogues of **9-NiY** were synthesized (**10-NiY**, **11-NiY** and **12-NiY**) with modified organic ligands (Chart 3, H_2**L10**, H_2**L11** and H_2**L12**) and the general formula $[Ni^{II}_2Dy^{III}_2(\mathbf{LX})_4(DMF)_2]$ determined by X-ray crystallography. In a comparative study, **9-NiDy** and all the **X-NiY** catalysts were all used to test the scope of reaction with a variety of primary and secondary amines. **9-NiY** was found to be the best catalyst for this reaction with

both secondary and primary amines (Table 9). Modification of the organic periphery appeared to have an insignificant effect on the catalytic yield of product. An attempt to form an isostructural 3d-4f heterogenous catalyst instead of a homogenous one, derived from H_2**L13**, was unsuccessful.

Table 9. Comparative study to determine the structure-activity relationships for **X-NiLn** catalysts with modified ligands.

	Compound	**9-NiDy**	**9-NiY**	**10-NiY**	**11-NiY**	**12-NiY**
	Loading/ %	1	0.5	1	0.5	1
	Time/h	16	8	12	8	12
Entry	Product	Yield/ %	Yield/ %	Yield/ %	Yield/ %	Yield/ %
1	$O(CH_2CH_2)_2NH$	Quantitative	Quantitative	91	Quantitative	85
2	$(CH_2{=}CHCH_2)_2NH$	99	96	85	95	80
3	C_8H_9N	95	99	70	94	64
4	$C_9H_{11}N$	61	53	58	51	52
5	*Iso*-$C_9H_{11}N$	63	71	69	69	62
6	$C_6H_5NH_2$	96	99	96	99	94
7	$CH_3OC_6H_4NH_2$	62	91	91	93	91
8	$FC_6H_4NH_2$	70	95	94	94	92
9	$CF_3C_6H_4NH_2$	26	90	81	86	81

Overall, these results suggest that the above described well characterised Ni/4f catalysts promote the transformation of *trans*-4,5-diaminocyclopent-2-enones from 2-furaldehyde and secondary and primary amines. Their catalytic efficacy is comparable or even better with that of the expensive $Sc(OTf)_3$ or the recently reported microwave methodology.[83–86] Interestingly, a recent report demonstrated that *trans*-4,5-diamino-cyclopent-2-enones can be formed in aqueous solution with a $Cu(OTf)_2$ catalyst,[89] instead of in traditional organic solvents. This observation and the mild catalytic conditions present a natural pathway to further develop this catalytic system and to develop water soluble 3d-4f CCs.

2.2.3 Zn^{II}/Ln^{III} CCs in Friedel-Crafts reactions

Following the successful venture of our first tetranuclear 3d-4f CC catalysts in the domino/electrocyclization reaction several important considerations had been demonstrated; the Ln^{III} ion could be substituted; the coordination environment of Ln^{III} and M^{II} could be altered and Schiff base ligand could be modified. These factors could lead to improved catalytic behaviour of the 3d-4f CC. However, up to this point we had determined little of the mechanistic action of 3d-4f CC catalysis and the role of the 3d ion had been effectively inert.

With these deficiencies in mind we attempted to synthesise Zn^{II} analogues of **9-NiLn,** to act as co-operative catalysts, as it had been previously shown both Ln^{III}, Zn^{II} salts with Schiff base ligands had successfully catalysed Friedel-Crafts (FC) alkylation reactions.[90,91] In addition, the diamagnetic Zn^{II} ion would allow study of various Ln^{III} analogues by EPR or ^{1}H NMR. Our next publication attempted to address these issues.[92] Though an attempt to synthesise isostructural Zn^{II} analogues of **9-NiLn** was not successful, a modified reaction procedure gave a family of eight novel isoskeletal $[Zn^{II}_2Ln^{III}_2(\mathbf{L9})_4(NO_3)_2(DMF)_2]$ (**13-ZnLn**, Figure 7) (Ln = Sm, Eu, Gd, Tb, Dy, Yb or Y) CCs which possess a defect dicubane topology.

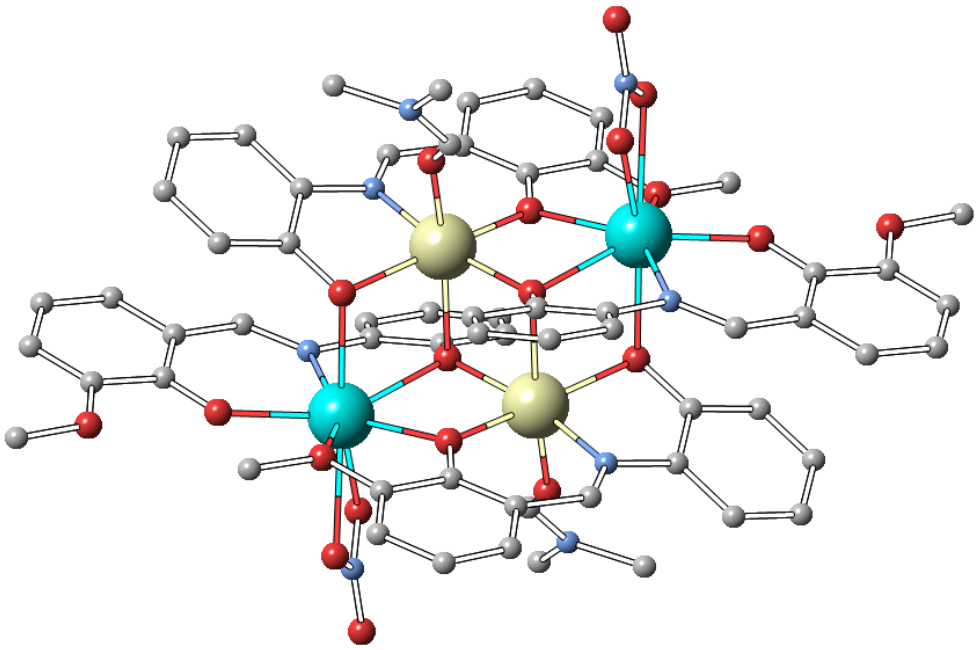

Figure 7. Molecular structure of **13-ZnLn**. Colour code: Ln^{III}, light blue; Zn^{II}, pale yellow; O, red; C, grey and N, pale blue. Hydrogen ions omitted for clarity.

A range of spectroscopic evidence indicates that the defect dicubane topology is retained in solution. First, ESI-MS, shows two prominent peaks, indicative of $[Zn^{II}_2Ln^{III}_2(\mathbf{L9})_4(NO_3)]^{+}$ and $[Zn^{II}_2Ln^{III}_2(\mathbf{L9})_4(MeOH)]^{2+}$ fragments, indicating that the core is stable in solution. In ^{1}H NMR spectra the peak areas for the imine, aromatic, and methoxy protons are all consistent with the structure as determined by X-ray crystallography. However, further analysis proved difficult due to asymmetry, dynamic behaviour, and low solubility. For further confirmation of the solution stability of **13-ZnLn**, Q-band EPR spectra of **13-ZnGd** in both solid and solution phase were recorded. These confirm that the spectra arise from $S = 7/2$ Gd^{III} ions with rhombic zero-field splitting (ZFS) and the highly sensitive, finger-print-like ZFS of the $S = 7/2$ state

signal directly indicates that the coordination environment of the Gd^{III} ion is unchanged in solution.

The catalytic behaviour of this series was initially probed with the FC alkylation of indoles with aldehydes to bisindolylmethanes (BIMs)[92] and indoles with nitrostyrenes.[93] All **13-ZnLn** CCs display good catalytic efficacy for the synthesis of BIMs (Table 10, entries 2-8) at 2.5 mol% loading. The Y^{III} (**13-ZnY**) analogue surpasses the performance of the corresponding triflate salt and all other Ln^{III} analogues and a 96% yield can be obtained with a loading of only 1 mol%. Subsequent optimisation proves that the presence of H_2O is crucial to obtain high yields and no conversion to product is observed solvents of low polarity.

Table 10. Optimisation of the FC alkylation of indole with benzaldehyde catalysed by **13-ZnLn** CCs.

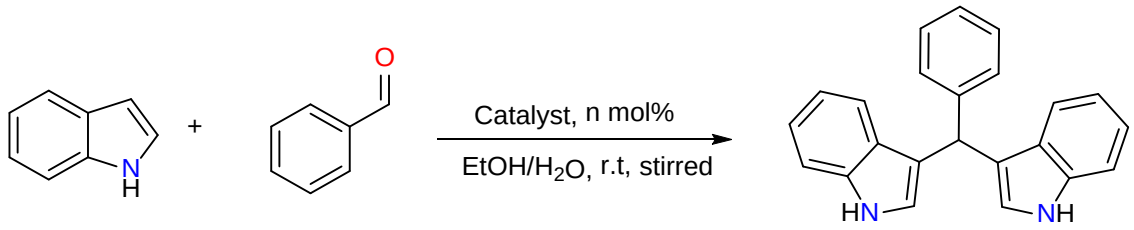

Entries	Catalyst	T	Loading/ mol%	Time/ h	Yield/ %
1	None	r.t	2.5	12	0
2	**13-ZnDy**	r.t	2.5	12	92
3	**13-ZnY**	r.t	2.5	12	quantitative
4	**13-ZnSm**	r.t	2.5	12	87
5	**13-ZnEu**	r.t	2.5	12	53
6	**13-ZnTb**	r.t	2.5	12	80
7	**13-ZnGd**	r.t	2.5	12	75
8	**13-ZnYb**	r.t	2.5	12	94
9	**13-ZnY**	r.t	1	12	96

In contrast, the FC alkylation of indoles with nitrostyrene, the early Ln^{III} analogues showed a much-reduced efficacy (Table 11, entries 4 - 7), but the Dy^{III}, Yb^{III} and Y^{IIII} analogues yields gave significantly higher yields (Table 11, entries 2 - 3). Unlike the previous example, the presence of H_2O was not essential to obtain high yields and solvents of higher polarity were as effective. Catalyst loadings could be reduced to 1 mol%. The yields for product for both

increased as the size of lanthanide contracted, indicating Dy^{III} or Yb^{III} may be a "sweet spot" for 3d-4f CC catalysed FC reactions.

Table 11. Optimisation of the FC alkylation of indole with *trans*-β-nitrostyrene catalysed by **13-ZnLn** CCs.

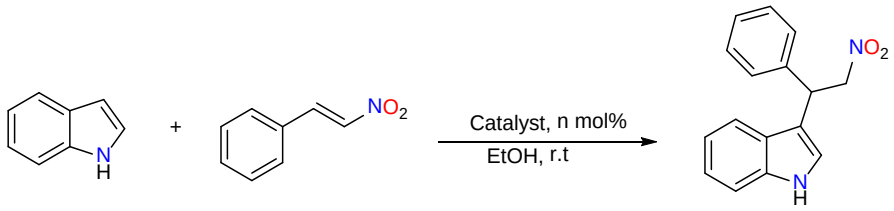

Entries	Catalyst	T	Loading/ mol%	Time/ h	Yield/ %
1	none	r.t	1	24	0
2	**13-ZnDy**	r.t	1	24	99
3	**13-ZnY**	r.t	1	24	94
4	**13-ZnEu**	r.t	1	24	55
5	**13-ZnGd**	r.t	1	24	30
6	**13-ZnNd**	r.t	1	24	12
7	**13-ZnTb**	r.t	0.5	24	24

The scope of each reaction was extended. The alkylation of indoles with aldehydes and the **13-ZnY** catalyst gave very good to excellent yields (Scheme 8). However, when ketones were used in the place of aldehydes, long reaction times were necessary to give low yields of the desired product. This behaviour recalls the selective reduction of ketones in the presence of aldehydes (Luche reaction).[94] N-methyl-indole and indole-3-acetic acid do not react with benzaldehyde indicating that a) if the most active site (C-3) of the indole group is blocked the reaction does not proceed and b) coordination of the nitrogen atom is crucial.

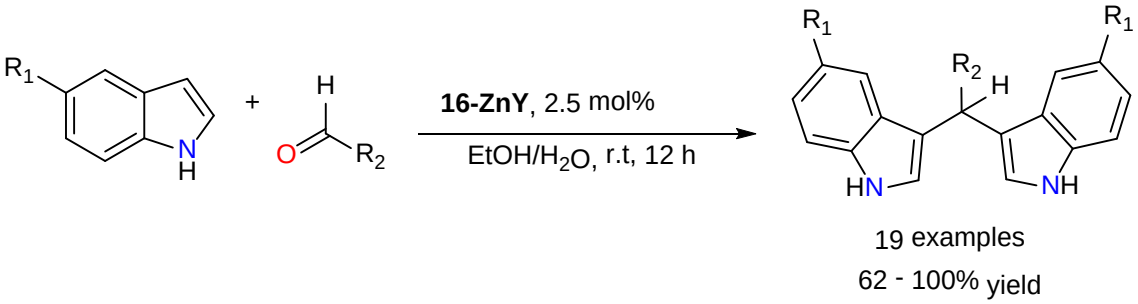

Scheme 8. Scope of the **13-ZnY** catalysed FC reaction to form BIMs.

To explore the scope of the FC alkylation of indole with *trans*-β-nitrostyrene, various nitroalkenes were treated with indoles and the **13-ZnDy** catalyst (Scheme 9). With R^2 as aromatic, several catalytic systems gave slightly lower yields due to the electronic effect of para substitution of the phenyl group of aromatic nitroalkenes. In all these cases, very good yields were obtained. The effect of substitution of the indole at position at 5 of the indole had little effect on the yield except for the electron-drawing group. Reactions between N-alkylated or 2-methyl indole and various nitrostyrenes gave isolated products in good to excellent yields. A change of the substituent at the nitrogen atom in position 5, and at the 2-position of indole did not show any profound effect on the yield of the desired product.

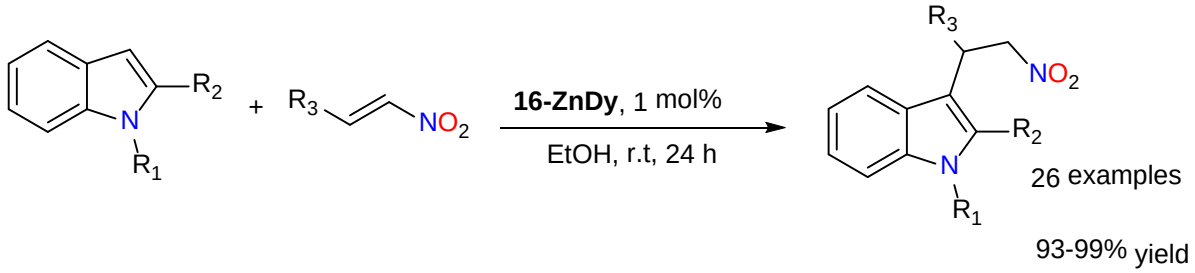

Scheme 9. Scope of the FC alkylation of Indoles with various nitrostyrenes catalysed by **13-ZnDy**.

UV-Vis binding studies for the **13-ZnLn** series gave information regarding the reaction mechanism and whether substrates were indeed binding or interacting with the $Zn^{II}_2Ln^{II}_2$ core. Initial studies were conducted with 2-napthaldehyde showed that the intensities of the peak at 290 nm for 2-napthaldehyde gradually decreased with time with the addition of **13-ZnDy** indicating weak van de Waals interactions between the substrate and CC. Similar behaviour was observed with indole for both FC reactions. Similar studies were conducted with $Zn(OTf)_2$ and $Dy(OTf)_3$ to determine the preference of each substrate for the Ln^{III} or the Zn^{II} metal centres. Results suggested that 2-napthaldhyde preferentially binds to the Dy^{III} centre and Indole to Zn^{II}. Similar behaviour is identified with nitroalkanes, where there is suspected preference for the Dy^{III} centre. The **13-ZnDy** catalyst with all substrates demonstrated a greater rate of quenching than either $Zn(OTf)_2$ and $Dy(OTf)_3$, which perhaps indicates a stronger interaction with the metal centres in tandem.

Our most recent report details the synthesis and characterisation of dinuclear 3d-4f CCs, from H_2**L3**, which are isoskeletal to the species hypothesised by Shibasaki (**1-CuSm**).[95] This work highlights the problems associated with the *in situ* synthesis of 3d-4f CCs for catalysis. Though the $[Zn^{II}Ln^{III}$(**L3**)$Cl_3]$ and $[Zn^{II}Ln^{III}$(**L3**)$(NO_3)_3]$ species were targeted, four CCs with

the general formulas $[Zn^{II}_2Dy^{III}_2$(**L3**)$_2(CO_3)_2(NO_3)_2]$ (**14-ZnDy**), $[Zn^{II}Y^{III}$(**L3**)$(NO_3)_2$(o-van)(MeOH)]·MeOH (**15-ZnY**) and $[Zn^{II}Ln^{III}$(**L3**)$(NO_3)_2$Cl(EtOH)], where Ln = Dy (**16-ZnDy**) and Y(**16-ZnY**), were isolated and characterised by X-ray diffraction studies (Figure 8). The synthetic conditions for these compounds are shown in Table 12. The synthesis of **14-ZnDy** and **15-ZnY** follows a two-step procedure where H_2**L3** is refluxed in ethanol solution with $Zn(OAc)_2·4H_2O$ to form a Zn**L3** metalloligand which is shown in Scheme 10. Zn**L3** was then subsequently reacted in MeOH with $Ln(NO_3)_3$ to form each respective CC upon slow evaporation (SE). The synthesis of both **16-ZnLn** relies upon a mixed one-pot solution of the reactants, solvent and reaction ratios shown in Table 12 followed by SE.

Unexpected structural motifs were identified in the isolated species. Despite Y^{III} having a similar ionic radius with Dy^{III}, the analogous reactions yield the tetranuclear species 1**4-ZnDy** and the dinuclear 1**5-ZnY** where an oxophilic o-vanillin fulfils the vacant positions of coordination sphere of the Y^{III} centre. Unfortunately, it was not possible to synthesise the **6-ZnLn** CCs with only $[Cl]^-$ counter ions. ESI-MS studies for **14-ZnDy** and **15-ZnY** displayed peaks in the MS (positive-ion mode) which corresponded to the general fragment formula $[Zn^{II}Ln^{III}$(**L3**)$(NO_3)_2]$. This indicates that the tetranuclear unit of **14-ZnDy** dissociates in solution and forms the corresponding dinuclear moieties. **16-ZnLn** displayed peaks in the MS (positive-ion mode) which corresponded to the general fragment formula $[Zn^{II}Ln^{III}$(**L3**)$Cl(H_2O)_2]^+$, indicating that the dinuclear core is retained when solubilised. In conjunction, the solid and solution state characterisation highlights the difficulty of targeting 3d-4f CCs of a specific structure and especially identifying their exact dinuclear structure in *in situ* catalytic reactions.

Table 12. Conditions for the synthesis of 1**4-ZnDy**, 1**5-ZnY** and **16-ZnLn** CCs.

Entry	General formula	Ln^{III} source	M^{II} source	Ligand	Solvent	Ratio (Ln:M:H_2**L3**)	Crystallisation method
1	$[Zn^{II}_2Dy^{III}_2$(**L3**)$_2(CO_3)_2(NO_3)_2]$ (**14-ZnDy**)	$Dy(NO_3)_3·5H_2O$	Zn**L3**	Zn**L3**	MeOH	1:-:1	SE
2	$[Zn^{II}Y^{III}$(**L3**)$(NO_3)_2$(o-van)(MeOH)]·MeOH (**15-ZnY**)	$Y(NO_3)_3·5H_2O$	Zn**L3**	Zn**L3**	MeOH	1:-:1	SE
3	$[Zn^{II}Ln^{III}$(**L3**)$(NO_3)_2$Cl(EtOH)] (**16-ZnLn**) Ln = Dy, Y	$Y(Cl_3)·xH_2O$	$Zn(NO_3)_2·6H_2O$	H_2**L3**	EtOH	1:1:1	SE

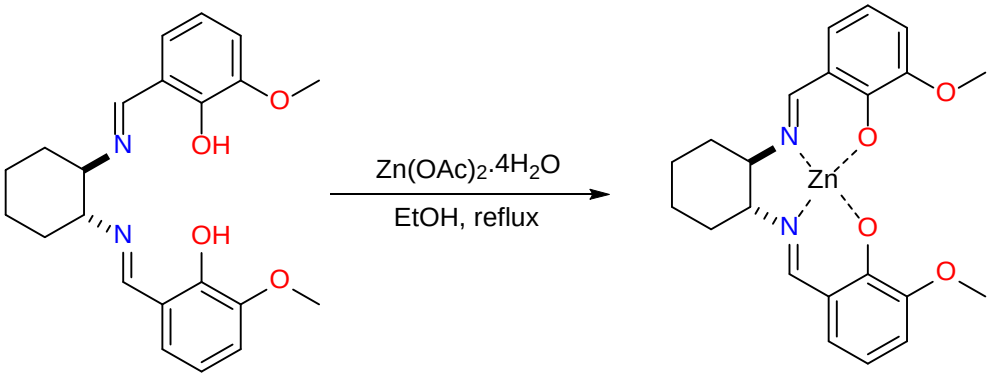

H_2**L3** ZnL3

Scheme 10. The preparation of Zn**L3**.

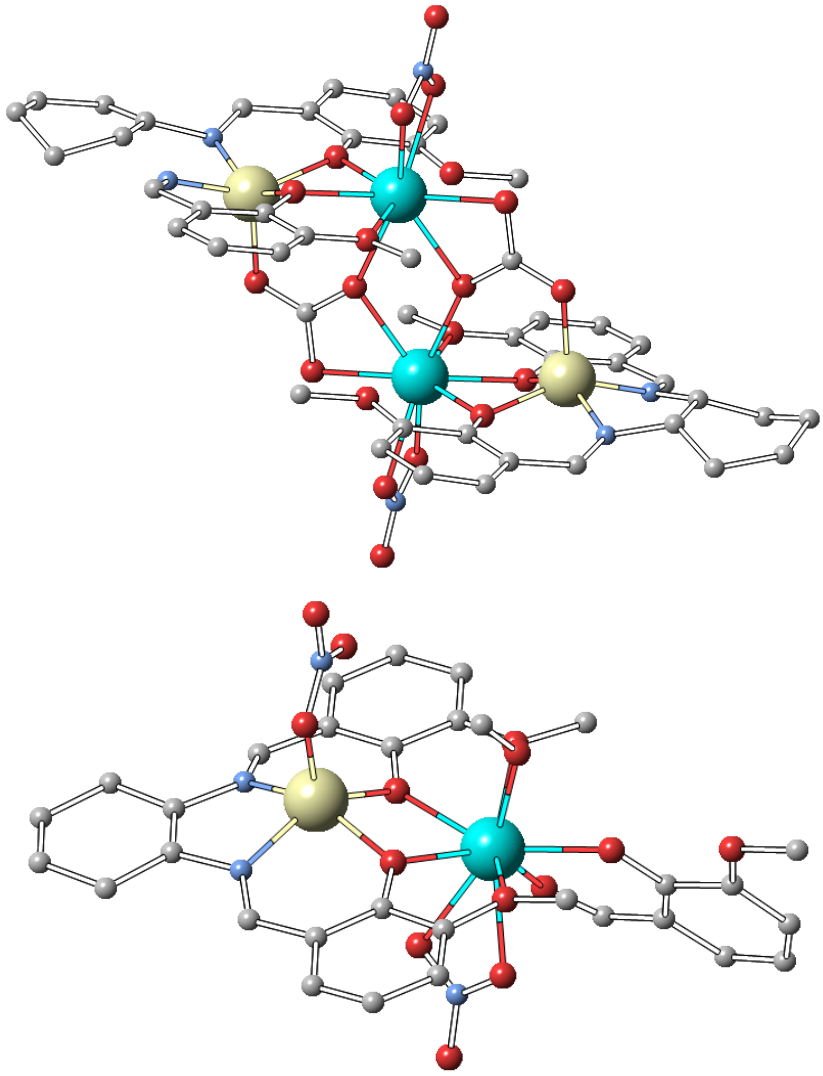

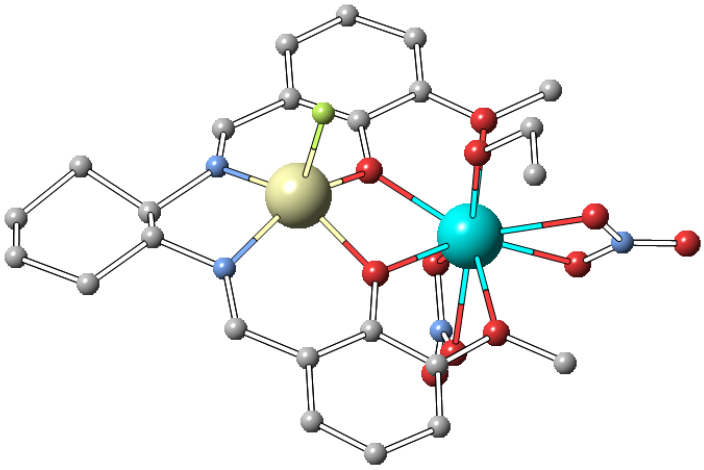

Figure 8. Molecular Structures of **14-ZnDy** (upper), **15-ZnY** (middle) and **16-ZnLn** (lower). Colour code: Ln^{III}, light blue; Zn^{II}, pale yellow; O, red; C, grey, Cl, pale green and N, pale blue. Hydrogen ions and counter ions are omitted for clarity.

Table 13. Benchmarking studies for the addition of 5-methoxyindole to α, β-unsaturated 2-acyl imidazole catalysed by **14-16-ZnLn**.

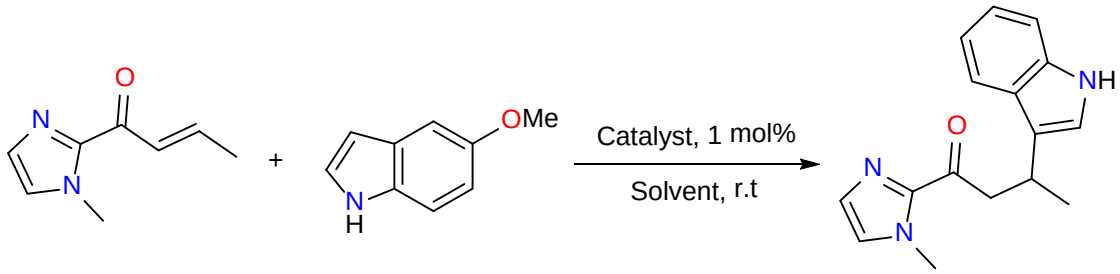

Entry	Catalyst	Solvent	Time/ days	Yield/ %
1	-	MeCN	3	-
2	Cu/dmbpy	MeCN	1	96
3	**14-ZnDy**	MeCN	3	18
4	**14-ZnDy**	MeOH	2	40
5	**14-ZnDy**	EtOAc	4	41
6	**15-ZnY**	EtOAc	3	99
7	**16-ZnDy**	EtOAc	3	90
8	**16-ZnY**	EtOAc	3	47

Initially, the **14-16-ZnLn** CCs were evaluated as catalysts for the addition of 5-methoxyindole to α, β-unsaturated 2-acyl imidazole (Table 13). The performance of **14-ZnDy** was compared to copper nitrate/ 4,4'-dimethyl-2,2'-bipyridine (Cu/dmbpy), with a 1 mol% loading of

catalysts in MeCN, which is a common catalytic system for this transformation. Cu/dmbpy significantly out-competed **14-ZnDy** (Table 13, entry 2 v 3), while in MeOH the yield of product increased (Table 13, entry 4) but the MeO addition by-product was also observed to form. The use of EtOAc eliminated by-product formation and resulted in a 41% yield of the Friedel-Crafts product (Table 13, entry 5). With the optimised conditions the rest of the Zn^{II}-Ln^{III} CCs were tested as catalysts and displayed a much-improved performance over **14-ZnDy** (Table 13, entries 5 - 8). The Y^{III} containing compounds showed a slightly higher catalytic activity than the Dy^{III} derivatives, pre-catalyst **15-ZnY** being the most effective (Table 13, entry 6). This may indicate that the efficacy of the CCs is highly dependent on the coordination environment around the Y^{III} and Dy^{III} ions.

15-ZnY was used to further investigate the scope of reaction. The substitution of the electron withdrawing groups on the indole resulted in a substantial reduction in conversion of substrates to product, whereas the conjugate addition of N-methyl indole resulted in an almost quantitative yield of product (Scheme 11). The replacement of indoles with other types of nucleophiles (e.g. 1.3-dioxane-4,6-dione and dimethyl malonate) resulted in corresponding products in good yields (67 – 100%).

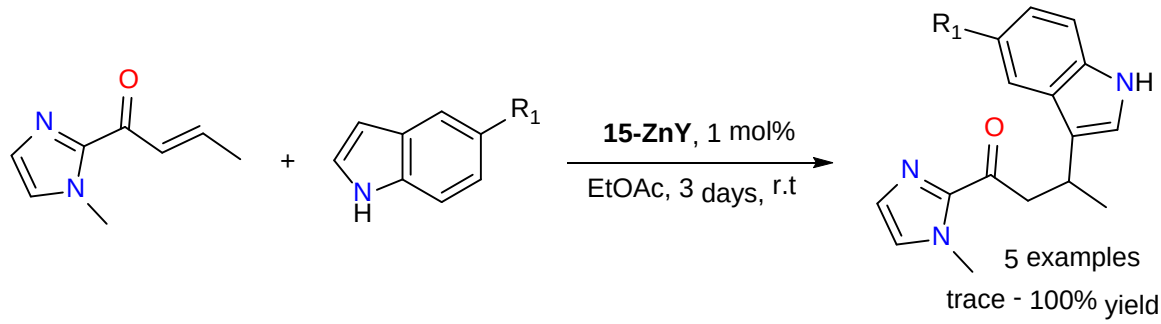

Scheme 11. Scope of the FC alkylation of various indoles with α, β-unsaturated 2-acyl imidazole catalysed by **15-ZnY**.

Overall, these results suggest that *in situ* synthesised catalysts for catalytic screenings is not a good practice as it overlooks the possible formation of multiple 3d/4f species that may influence the observed catalytic behaviour. The well characterized 3d/4f CCs can promote the transformation in almost an order of magnitude less loading when compared with metal salts. The importance of the coordination environment around the dinuclear metal core is also emphasised for the first time with 3d-4f CC catalysts.

2.2.4 Tetranuclear $Zn^{II}_2Ln^{III}_2$ CCs for the multicomponent Petasis Borono-Mannich reaction

The demonstration that **13-ZnLn** is an effective catalyst for FC alkylation led us to examine several further reactions.[92,93] The chelation of aldehydes to Ln^{III}/Y^{III} metals, shown by UV-studies, suggested that these catalysts would be an ideal synergistic template for multicomponent reactions.[96]The Petasis borono-Mannich (PBR) reaction, with the specific substrates shown (Scheme 12) yields in a single step aminophenol derivatives which are suitable for the preparation of dihydro-1,3-oxazines, triaryl-methanes and polycyclic acetals. However, previous reaction procedures suffered from several disadvantages and required high temperatures, high catalyst loadings and long reaction times.

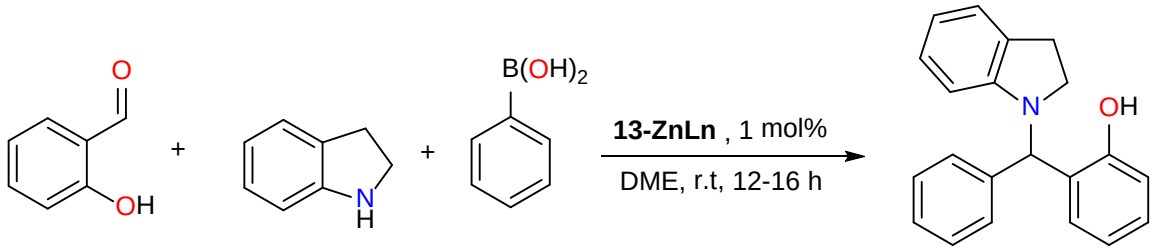

Scheme 12. Optimisation of the Ln^{III} ion of the **13-ZnLn** catalysed Petasis Borono-Mannich reaction.

Initial optimization of reaction conditions carried out with **13-ZnDy**, showed that DME is the most effective solvent for catalysis of the reaction at room temperature, whereas many other polar and non-polar solvents showed an inhibitory influence. An increase in catalyst loading beyond 1 mol% led to a lower yield of the desired product. Other catalysts in the $Zn^{II}_2Ln^{III}_2$ series (**13-ZnLn**) were then examined. The results are summarized in Table 14. The desired product was obtained in moderate to excellent yields. A control experiment in the absence of the 3d-4f CCs catalyst showed 40% conversion (Table 14, entry 1). Moderate conversions were obtained in the presence of Dy or Zn salts (Table 14, entries 2-3). **13-ZnDy** and **13-ZnY** showed higher activity than **13-ZnGd**, **13-ZnEu**, **13-ZnYb** and **13-ZnTb** (Table 14, entries 4 - 9).

Table 14. Optimization of the PBR with **13-ZnLn**.

Entry	Loading/ mol%	Catalyst	Yield/ %
1	N/A	None	40
2	1	$Zn(OTf)_2$	46
3	1	$Dy(OTf)_3$	36
4	1	**13-ZnY**	74
5	1	**13-ZnNd**	55
6	1	**13-ZnGd**	54
7	1	**13-ZnDy**	96
8	1	**13-ZnTb**	66
9	1	**13-ZnYb**	57

To demonstrate the applicability of the optimised reaction conditions, different secondary amines, aldehydes and boronic acids were employed in the PBR, using **13-ZnDy** as catalyst (Scheme 13). The reaction proceeds in very good to excellent yields at room temperature with catalyst loading of 1.0 mol%. Very good yields were obtained with indoline as secondary amine, and reactions with *N*-methylaniline, and *N*-benzyl methylamine, gave very good yields. The presence of an electron donating group in the *para*-position of the boronic acid gives the corresponding product in very good yields, whereas the nature of secondary amine influences the total yield. The PBR between salicylic aldehyde or *o*-vanillin, secondary amines and benzene 1, 4-diboronic acid afforded products in very good yields (Scheme 13). From an extensive literature review, it is thought that this is the first time that benzene 1,4-diboronic acid is successfully involved in the titled reaction. The reaction does not proceed with the use of primary amines or benzaldehyde indicating the importance of the hydroxyl group in the aldehyde to activate the boronic acid.[31]

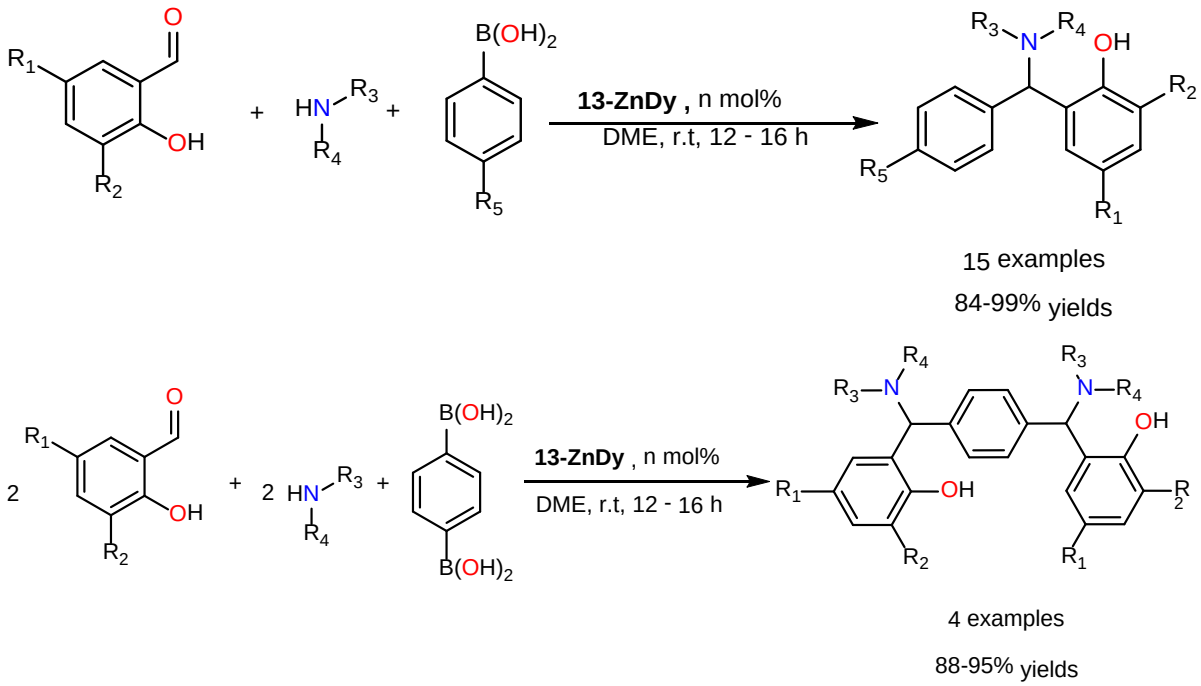

Scheme 13. Scope of the **13-ZnDy** catalysed Petasis borono-Mannich reaction.

Though the 4f centres were changed without altering the core topology, it was not possible to study the *in situ* catalytic reaction via ^{1}H NMR spectroscopy with **13-ZnY** due to the insolubility of this type of catalyst.

2.2.5 Isoskeletal $Zn^{II}_2Ln^{III}_2$ CCs for the mechanistic study of a Michael Addition Reaction

Mechanistic aspects of the use of **13-ZnLn** CCs as catalysts were explored in a comprehensive study of the Michael addition (MA) between 1, 3-dimethyl barbituric acid and *trans*-β-nitrostyrene.[97] This reaction has received significant attention due to the potential of the final products.[98–102] After initial optimisation of the reaction conditions, **13-ZnLn** (Ln = Sm, Eu, Tb, Gd or Dy) Table 15, entries 2 – 6 were found to give moderate performance. However, the use of **13-ZnY** and **13-ZnYb** led to the MA in quantitative yield within 15 min at room temperature (Table 15, entries 7 and 8).

Table 15. Optimisation of Ln^{III} ion of **13-ZnLn** catalysts towards the MA reaction between 1,3-dimethyl barbituric acid and *trans*-β-nitrostyrene.

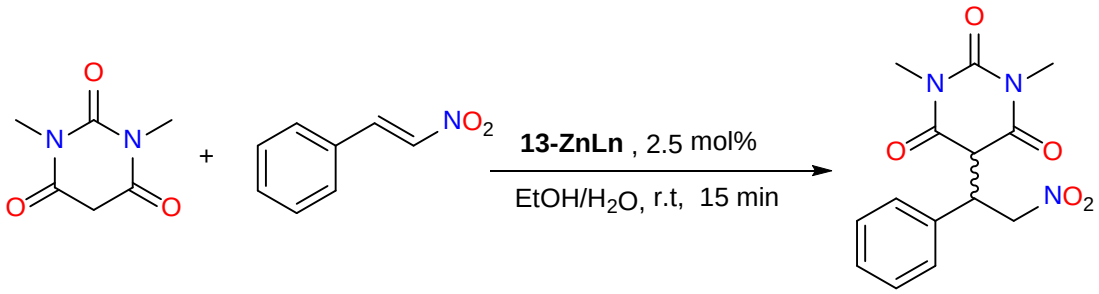

Entry	Loading/ %	Catalyst	Yield/ %[b]	Time/ min
1	0	None	35	60
2	2.5	**13-ZnSm**	75	15
3	2.5	**13-ZnEu**	81	15
4	2.5	**13-ZnGd**	89	15
5	2.5	**13-ZnTb**	88	15
6	2.5	**13-ZnDy**	94	15
7	2.5	**13-ZnYb**	quantitative	15
8	2.5	**13-ZnY**	quantitative	15

To further understand the role of the metals in the **13-MLn** scaffold, we studied parallel reactions of the isoskeletal compounds **13-NiDy, 13-CoDy**, and **13-CuDy**. The reactions of **13-CuDy** and **13-ZnDy** yielded the desired product in very good yields (90%) but with **13-NiDy** and **13-CoDy** showed poor performance (Table 16). These differences can be rationalized by consideration of the Irving-William stability series, in which for a given ligand the stability of dipositive metal ion complexes increases in the order: $Co^{II} < Ni^{II} < Cu^{II} < Zn^{II}$. It was therefore apparent that binding (i.e., activation) of at least one of the substrates via an O atom to a 3d metal centre was required for efficient catalysis.

Table 16. Optimisation of M^{II} ion of **13-MLn** catalysts towards the MA reaction between 1,3-dimethyl barbituric acid and *trans*-β-nitrostyrene

Entry	**Loading / %**	**Catalyst**	**Yield/ %**	**Time/ min**
1	2.5	**13-ZnY**	quantitative	15
2	2.5	**13-ZnDy**	94	15
3	2.5	**13-NiDy**	29	15

4	2.5	**13-CoDy**	34	15
5	2.5	**13-CuDy**	85	15

The **13-ZnY** compound (Table 16, entry 1) was found to have the greatest efficacy (quantitative, 2.5 mol%). Therefore, Y^{III} and Zn^{II} ions were chosen to investigate the ligand structure-activity relationship. Twenty isoskeletal CCs with the general formula $[Zn^{II}_2Y^{III}_2(\mathbf{LX})_4(NO_3)_2(DMF)_2]$ (**LX**, Table 17) were synthesised in a procedure almost identical to that for **13-ZnY**. These were isoskeletal to **13-ZnY** and studies of the series by ESI-MS, EPR and ^{1}H NMR indicated that the defected dicubane topology was retained throughout.

Table 17. Ligands used for the synthesis of $[Zn^{II}_2Y^{III}_2(\mathbf{LX})_4(NO_3)_2(DMF)_2]$ CCs.

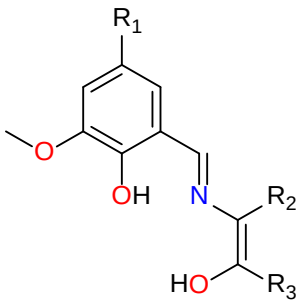

R_1	R_2 R_3						
	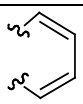	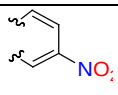	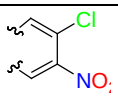	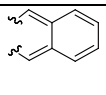	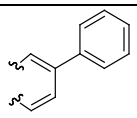	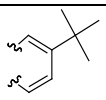	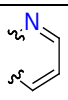
H	H_2**L9**	H_2**L15**	H_2**L18**	H_2**L11**	H_2**L22**	H_2**L25**	H_2**L28**
CH_2-CH=CH_2	H_2**L10**	H_2**L16**	H_2**L19**	H_2**L12**	H_2**L23**	H_2**L26**	H_2**L29**
Br	H_2**L14**	H_2**L17**	H_2**L20**	H_2**L21**	H_2**L24**	H_2**L27**	H_2**L30**

The catalysts with the ligands shown in Table 17 were used for MA and the ligand modification was found to have a noticeable effect on the efficacy of the catalytic reaction. **13-ZnY** (Table 17) was found to be the most catalytically effective (1 mol% loading, quantitative, 15 min) and the scope of reaction was expanded to a variety of substituted nitrostyrenes and Michael acceptors in good to excellent yields (Scheme 14).

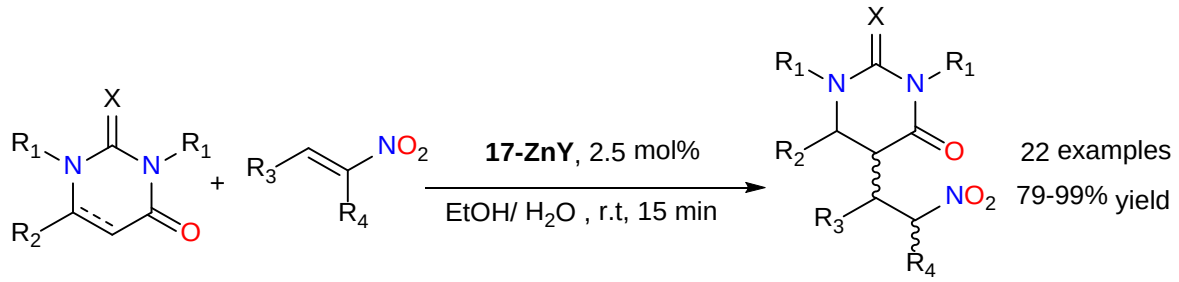

Scheme 14. Scope of the **32-ZnY** catalysed MA reaction.

When *trans*-β-methyl-nitrostyrene was employed instead of *trans*-β-nitrostyrene in the **13-ZnY** catalysed reaction with 1,3-dimetyl barbituric acid, ^{1}H NMR data showed the presence of only one diastereomer (>20:1 dr) which was confirmed by an X-ray structure determination (R*, R*), which was previously unobserved. Parallel reactions were conducted with the **13-MLn** series. The **13-ZnLn** series only showed slight differences in diastereoselectivity which may be attributed to the different ionic radii of the lanthanides. **13-CoDy**, **13-NiDy**, and **13-CuDy** as catalysts and observed that all three CCs gave ~20:1 *dr*s, but that **13-CoDy** and **13-NiDy** gave significantly lower yields (Table 18, entries 8–10). Reactions with *cis*- β-methyl-4-methoxy-nitrostyrene gave similar drs and yields.

Table 18. Tests for diastereoselectivity of **13-MLn** catalysts.

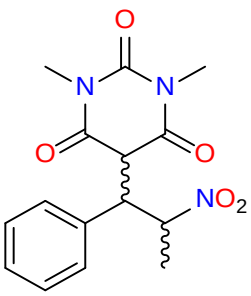

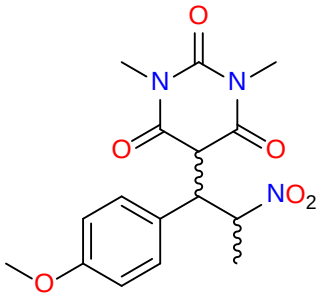

Entry	Catalyst	Yield/ %	dr (R*, R*/R*, S*)	Yield/ %	dr (R*, R*/R*, S*)
1	**13-ZnY**	quantitative	20:1	96	20:1
2	**13-ZnSm**	75	>20:1	69	>20:1
3	**13-ZnEu**	81	>20:1	74	>20:1
4	**13-ZnGd**	89	>20:1	77	>20:1
5	**13-ZnDy**	94	>20:1	89	>20:1
6	**13-ZnTb**	88	>20:1	85	>20:1

7	**13-ZnY**	quantitative	20:1	93	20:1
8	**13-CoDy**	24	20:1	41	20:1
9	**13-NiDy**	19	20:1	30	20:1
10	**13-CuDy**	71	20:1	94	20:1

The **13-ZnLn** system was studied by various techniques to examine substrate interaction with the CC core. ^{1}H NMR titration studies suggested that binding of individual substrates to the $M^{II}Ln^{III}$ complexes was not strong, but this did not impede catalytic action. Q-band EPR solution studies of **13-ZnGd** with the substrates in varying ratios showed slight differences in *g*-factors which were taken to indicate changes by the Gd^{III} coordination environment. However, we believed that the coordination number remains intact since the overall molecular symmetry is reflected in the experimental g-tensor. These results suggest that substrates interact with the $Zn^{II}{}_2Gd^{III}{}_2$ core without overall alteration of the CC. This substrate interaction was also supported by ESI-MS data on a sample taken during the reaction between *trans*-β-methyl nitrostyrene and barbituric acid catalysed by **13-ZnGd** gave peaks with *m*/*z* values that support the binding of the two substrates.

A plausible mechanism for the 3d-4f CC catalysed MA reaction between 1,3-dimethylbarbituric acid and *trans*-β-nitrostyrene was supported by DFT studies. The estimated binding energy of nitrate to the Y^{III} metal centre in aqueous solution in the tetranuclear species is 30.8 kcal/mol, therefore dissociation of seems to be difficult, however dissociation into the dinuclear species in solution seems more possible, which is supported by the previously ESI-MS substrate study. The binding of the barbiturate substrate to the Zn centre is very weak (estimated binding energy 2.8 kcal/mol). No interaction was observed with the Y^{III} centre. *Trans*-β-nitrostyrene derivatives showed a preference for coordination to Y^{III} centre of the Zn^{II}/Y^{III} catalyst with a unidentate coordination mode the estimated binding energy was predicted to be 4.3 kcal/mol. With these and other DFT calculations it was concluded that the barbiturate and *trans*-β- nitrostyrene substrates for the MA reaction catalysed by the $Zn^{II}Y^{III}$ bimetallic catalyst are co-operatively activated through their interaction with the Zn^{II} and Y^{III} metal centres of the catalyst.

2.2.6 3d-4f CC for carbon dioxide fixation

CO_2 is most widely abundant C1 building block and it is promising in transforming into various chemicals. One of the most attractive strategies is transforming CO_2 in various

cyclic carbonates which can be used in the production of engineering plastics and electrolyte solvents in lithium ion batteries.[103] Numerous metal complexes[104–106] have been reported as catalysts for the synthesis of cyclic carbonates and these include a number of heteronuclear catalysts including Zn^{II}-Mg^{II},[107] Zn^{II}-Ti^{II} [107] and $Zn^{II}_2Nd^{III}$.[108]

So far there have been two reports of 3d-4f CCs used as catalysts for the cycloaddition of styrene oxides and CO_2 to obtain cyclic carbonates.[109,110] The first of these described two isoskeletal heptanuclear 3d-4f CCs, which were synthesised from the "helical" H**L31** ligand (Chart 4), with the general formula $[Zn^{II}_4Ln^{III}_3(H\mathbf{L31})_4(NO_3)_8(H_2O)_2](NO_3)_2{\cdot}2H_2O$ (**37-ZnLn**) These are the largest nuclearity helicates among discrete 3d-4f CCs (Figure 9). The second report describes two series of tetra and hexanuclear Zn^{II}-Ln^{III} CCs, supported by the H**L32** Schiff base ligand (Chart 4), with the general formulas $[Zn^{II}_2Ln^{III}_2(\mu_3\text{-}OH)_2(\mathbf{L32})_4(NO_3)_4]$ (**38-ZnLn**) and $[Zn^{II}_4Ln^{III}_2(\mu_3\text{-}OH)_2(\mathbf{L32})_4(OAc)_6(NO_3)_2]$ (**39-ZnLn**) respectively are described (Figure 9). Single-crystal X-ray structural analysis and a variety of characterisation methods were used to confirm the structure of all these 3d-4f CCs and revealed the two metal centres of Ln and Zn were situated in the correct range to enable synergistic action as Lewis acid activators.

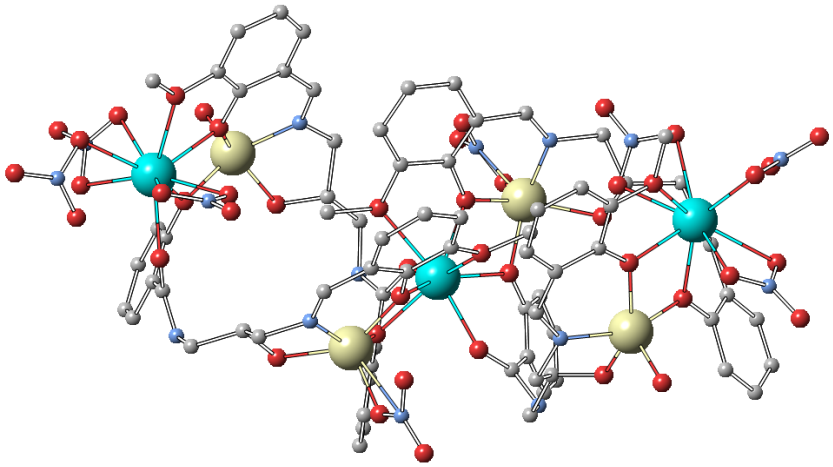

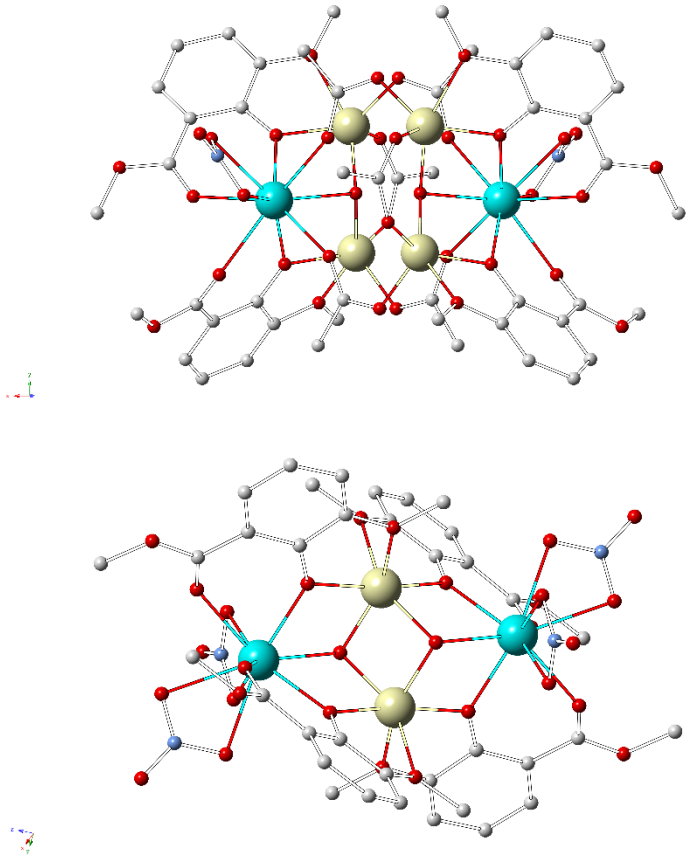

Figure 9. Molecular structure of **37-ZnLn**, **38-ZnLn** and **39-ZnLn.** Colour code: Ln^{III}, light blue; Zn^{II}, pale yellow; O, red; C, grey and N, pale blue. Hydrogen ions omitted for clarity.

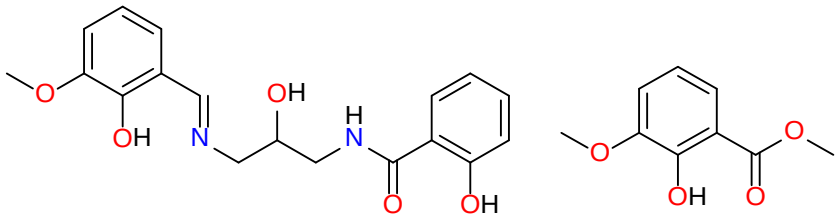

H_4**L31** HL**32**

Chart 4. Ligands used for the synthesis of 3d-4f CCs for carbon dioxide fixation.

Table 19. Synthesis of cyclic carbonate via the insertion of CO_2 intro styrene oxide catalysed by **37-ZnLn**.

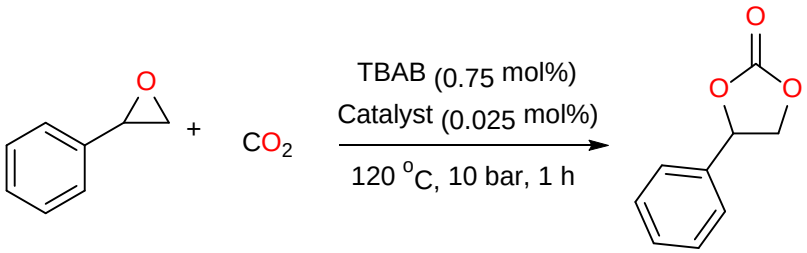

Entry	Catalyst	Co-catalyst	Yield/ %	TOF/ h^{-1}

1	-	Bu_4NBr	25	-
2	**37-ZnTb**	-	0	-
3	**37-ZnTb**	Bu_4NBr	96	3840
4	**37-ZnDy**	Bu_4NBr	95	3800
5	**37-ZnTb**	Bu_4NI	84	3360
6	**37-ZnTb**	Bu_4NCl	61	2440
7	**37-ZnTb**	Bu_4NBr	67	26,800

The initial catalytic investigation with **37-ZnLn** were performed for the cycloaddition of CO_2 to styrene oxide under solvent-free conditions with a tetrabutyl-ammonium bromide (TBAB) co-catalyst and both CCs afforded excellent yields of the corresponding cyclic carbonate (Table 19, entries 3 and 4). However, neither **37-ZnTb** nor TBAB alone could catalyse the reaction in good yields (Table 19, entries 1 and 2). The replacement of Tb^{III} (**37-ZnTb**) ions with Dy^{III} (**37-ZnDy**) ions only marginally decreased the yield and TOF of the catalytic product (Table 19, entries 3 and 4). Different co-catalysts were tested with Bu_4NBr being the best performer. The **37-ZnLn** CC catalysts exhibit a higher activity than previously reported Zn-salen[111,112] and lanthanide catalysts[105,106] and with optimised reaction conditions (Table 19, entry 7) displays a remarkably high TOF which is comparable to some of the best metal catalysts used for this polymerisation,[113–115] suggesting that the highly efficiency is due to the heterometallic catalyst system

Table 20. Synthesis of cyclic carbonate via the insertion of CO_2 intro styrene oxide catalysed by **38-ZnLn** and **39-ZnLn**.

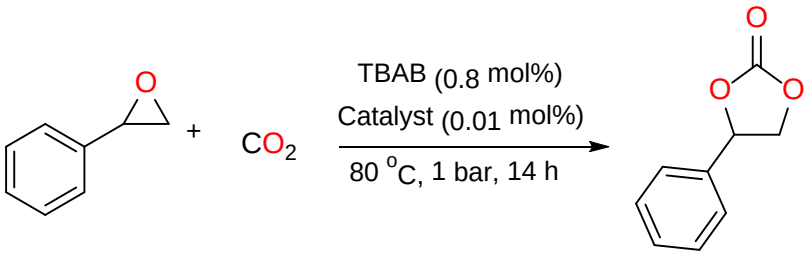

Entry	Catalyst	Temperature/ K	Yield/ %	TOF/ h^{-1}
1	**38-ZnEu**	80	0	0
2	**TBAB**	80	36	257
3	**38-ZnEu**	80	90	642
4	**38-ZnTb**	80	93	661

5	**38-ZnEr**	80	92	655
6	**38-ZnYb**	80	90	642
7	**38-ZnNd**	80	88	628
8	**39-ZnTb**	80	94	668
9	**39-ZnNd**	80	86	607

Similar screening studies were performed with **38-ZnLn** and **39-ZnLn** CCs, albeit with more mild reaction conditions. The cycloaddition of CO_2 to styrene oxide was first examined by using 0.01 mol% of **38-ZnLn** and **39-ZnLn** as catalysts and 0.8 mol% of TBAB as a co-catalyst under solvent-free conditions. In all circumstances, the cyclic carbonate was formed in good to excellent conversions with > 99 % selectivity (Table 20). Although TOF values were higher than previous MOFs, 3d and 4f complexes, they were significantly less than the **37-ZnLn** CCs (Table 20, entries 3 and 4), this may be due to the mild catalytic conditions. As with the previous study the Tb^{III} analogues were the most active (Table 20, entries 4 and 8) and the efficacy of lanthanide catalysts decreased either side of the period. Varying the co-catalyst or temperature had a detrimental effect on the yield and TOF, whereas increasing the CO_2 had no effect.

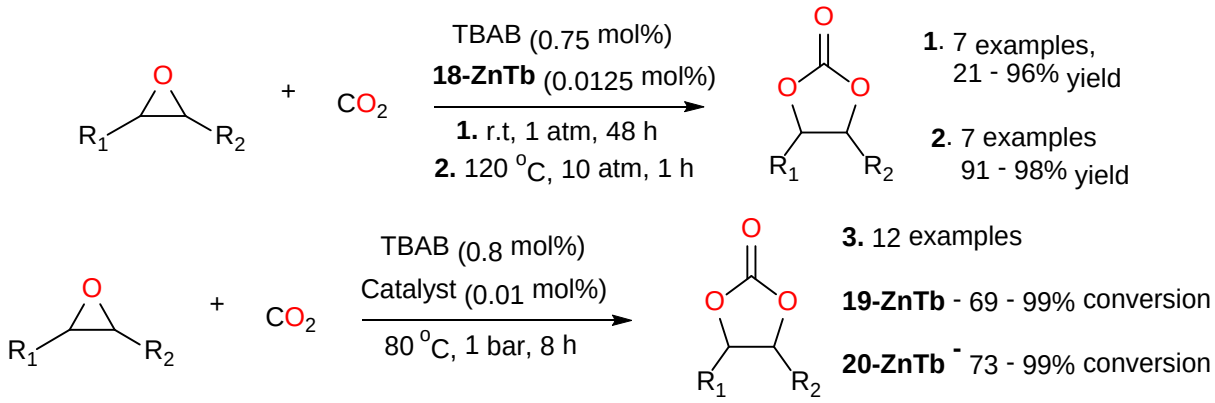

Scheme 15. Scope of the **37-ZnTb** catalysed carbon dioxide fixation of epoxides to carbonates.

The scope of the reaction system was extended to mono-substituted terminal epoxides with internal epoxide substrates, with the optimised reaction conditions and **37-ZnTb** (Scheme 15). All functionalised terminal epoxides were obtained in excellent yields, whereas internal epoxides exhibited a lower activity when compared to their terminal counterparts which was attributed to steric effects (Scheme 15, **1**). However good yields could be reached with an increased catalyst loading and long reaction time (Scheme 15, **2**).

The scope of the cycloaddition was tested with **38-ZnTb** and **39-ZnTb** and relatively high boiling point epoxide substrates were used to test the reactions at atmospheric pressure under solvent-free condition. Terminal epoxide substrates could be converted to the corresponding cyclic carbonates with high conversions (> 90%) and excellent selectivity (99%) (Scheme 15, **3**). Importantly, longer chain substrates such as 1,2-epoxypropane, glycidol, and glycidyl isopropyl ether converted to their corresponding cyclic carbonates in excellent conversions and selectivity. As for the internal epoxide, such as cyclohexene oxide, gives low conversions of only 20 % and 15 % by using **38-ZnTb** and **39-ZnTb** as catalysts, respectively. However, the conversions increased to 69 % and 73 % when the reactions were taken under 10 bar CO_2 pressure.

The **37-39-ZnTb** CC catalysts were recyclable under the catalytic conditions. And could be easily removed from the reaction mixture by filtration and each CC retained the characteristic Tb^{III} UV excitation. Powder X-ray diffraction and IR spectra provide further confirmation that all catalysts remain stable in up to five reaction cycles.

2.2.7 3d-4f CCs as vehicles in oxidation reactions

The previously described 3d-4f CC catalysts have all been concentrated on promoting organic transformation reactions, however a few water oxidation catalysts (WOCs) have been recently reported (Figure 10). These WOCs are a well characterised class of CC with cores based on the Mn_4Ca core of the oxygen evolving complex (OEC) involved in Photosystem II.[116] There are numerous homometallic binuclear transition metal complexes including Co_4,[117] Mn_4,[118] Mn_2,[119–121] Fe_2,[122–124,125] and Co^{III}_2[126] which mimic the water oxidation behaviour of OEC. Molecular mimics of the Mn_4Ca core have been reported with water oxidation properties including a Mn^{III}_3CaNa cluster based on a Schiff base ligand by Reedijk.[127] The synthesis of these oxidation catalysts has usually been based on previously reported compounds, such as the Mn_4Ca core or because of the multiple high oxidation state 3d and 4f metals which are found in them. However, the synthetic similarities between the three reported compounds are minimal as shown in Table 21.

Table 21. Synthetic conditions for the reported 3d-4f CC oxidation catalysts.

Entry	Formula	Ln^{III} salt	M^{II} salt	Ligand	Solvent	Ratio (Ln:M:L:Et$_3$N)	Crystallization method

1	$[CeMn_6O_9(\mathbf{L32})_9(NO_3)(H_2O)_2]$	$Ce(ClO_4)_4$	$[Mn(O_2CMe)_2]\cdot 4H_2O$	H**L3 2**	H_2O	2:2:3	SE
2	$[Co^{II}_3Ln^{III}(\mathbf{L33})_4(OAc)(H_2O)_5]$ (Ln = Ho, Er, Tm, Yb)	$Ln(OAc)_3$	$Co(Ac)_2\cdot 4H_2O$	H**L3 3**	THF	1:2:4	SE
3	$[(Fe^{III}Ce^{IV}O(\mathbf{L34})(NO_3)_4(H_2O)](ClO_4)$	$Ce(NO_3)_2$	$Fe(NO_3)_3$	**L34**	$MeCN/H_2O$	1:1:1	VD Et_2O
4	$[Mn^{II}Mn^{III}Ln^{III}_2(O_2CMe)_6$-$(H\mathbf{L35})_2(\mathbf{L36})](NO_3)\cdot H_2O$ Ln = Dy, Gd	$Ln(NO_3)_3$	$[Mn(O_2CMe)_2]\cdot 4H_2O$	H_2**L3 5**, H_2**L3 6**	MeOH/MeCN	1:1:2:4	SE

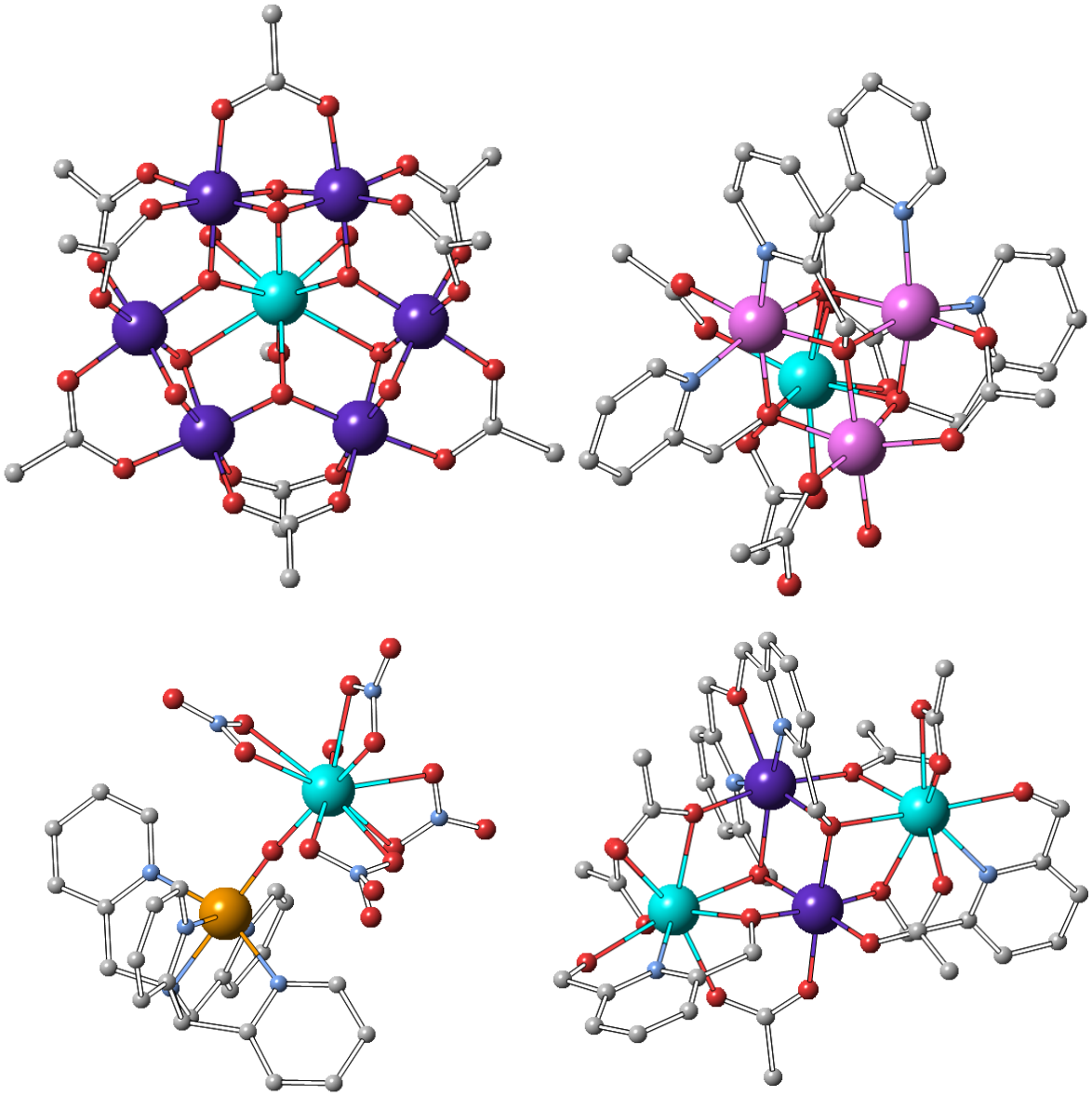

Figure 10. Molecular structure of 3d-4f CCs used as oxidation catalysts, **40-MnCe** (upper left), **41-CoLn** (upper right), **42-FeCe** (lower left) and **43-MnLn** (lower right). Colour code- Ln^{IV},

light blue; $Mn^{IV/III/II}$, purple; Fe^{III}, brown; Co^{II}, pink; O, red and C, grey; Hydrogen ions omitted for clarity.

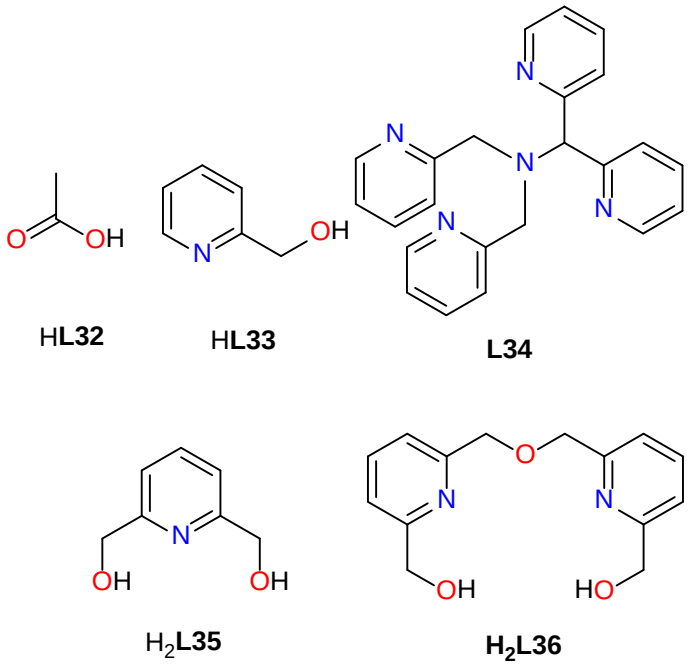

Chart 5. Ligands used for the synthesis of 3d-4f CC oxidation catalysts

Though not a WOC, the first example of a 3d-4f oxidation catalyst was a heptanuclear CC with the general formula $[Mn^{IV}_6Ce^{IV}O_9(\mathbf{L32})_9(NO_3)(H_2O)_2]$ (**40-MnCe**) (Figure 10) which was reported to catalyse the previously well explored oxidation of benzyl alcohol to benzaldehyde with a (2,2,6,6-tetramethylpiperidin-1-yl)oxidanyl (TEMPO) additive in with quantitative yields (Scheme 16).[128]

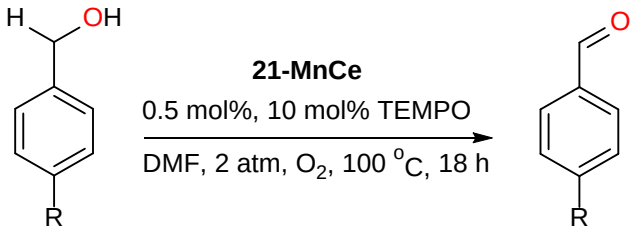

Scheme 16. The **40-MnCe** catalysed oxidation of benzyl alcohol to benzaldehyde.[128]

Initially, the aim of the study was to demonstrate the potential of $[Mn_{12}O_{12}(\mathbf{L32})_{16}(H_2O)_4]$ CCs as oxidation catalysts, due to the high oxidation state Mn^{III} and Mn^{IV} metal centres; ease of synthesis and well-defined structure of the CCs. The study was extended to mixed metal high-oxidation state metals (Ce^{IV}) and since both Mn^{IV} and Ce^{IV} are

strongly oxidizing, the possibility that their reduced forms generated by substrate oxidation could be reoxidised by O_2 suggested a potentially attractive catalytic system involving O_2 as the ultimate oxidant. Therefore, a previously synthesised 3d-4f CC with the general formula $[Mn^{IV}{}_6Ce^{IV}O_9(\mathbf{L32})_9(NO_3)(H_2O)_2]$ was employed. The **40-MnCe** CC was well characterised in the solid state, including by a single crystal X-ray diffraction study. In the TEMPO-assisted oxidation of $Ph(CH_2OH)$ with O_2 the **40-MnCe** CC catalyst (Table 22, entry 7) was significantly more efficient than the homometallic polynuclear Mn CCs with full conversion to product (Table 22, entry 1 - 6).

Table 22. Comparison of the **40-MnCe** with homonuclear $Mn^{III/IV}$ CC catalysts for oxidation of benzyl alcohol to benzaldehyde with a TEMPO additive.[128]

Entry	Catalyst	Catalyst loading/ mol %	TEMPO	Conversion to product / %
1	$[Mn_{12}O_{12}(\mathbf{L32})_{16}(H_2O)_4]$	1	22	62
2	$[Mn_{12}O_{12}(O_2CC_6H_4C_6H_5)_{16}(H_2O)_4]$	1	22	73
3	$[Mn_{12}O_{12}(O_2CC_6H_5)_{16}(H_2O)_4]$	1	22	64
4	$[Mn_{12}O_{12}(O_2CC_6H_4F)_{16}(H_2O)_4]$	1	22	80
5	$[Mn_3O(O_2CMe)_6(py)_3]$	1	22	72
6	$[Mn_4O_2(O_2CMe)_7(bpy)_2]$	1	22	76
7	**40-MnCe**	1	22	>99
8	**40-MnCe**	1	10	>99

With further optimisation it was possible to achieve near quantitative conversion with only 10 mol % of TEMPO (Table 22, entry 8). However, when these conditions were applied for the aerobic oxidation of *para*-substituted primary benzylic alcohols, 22 mol% TEMPO was required for quantitative conversion, indicating a significant substituent effect. Time-conversion plots demonstrated that the product did not decrease with time and FT-IR spectra of the recovered product is consistent with the starting material, suggesting the CC remains stable during reaction. The high efficiency of transformation could only be achieved when both high oxidation Ce^{IV} and Mn^{IV} were connected by oxide bridges and that homometallic CCs could not reach the same conversions.

More recently, a family of $Co^{II}_3Ln^{III}$ cubanes (Figure 10) with the general formula $[Co^{II}_3Ln^{III}(\mathbf{L33})_4(OAc)(H_2O)_5]$ (**41-CoLn**, where Ln = Ho, Er, Tm, Yb) were reported as the first 3d-4f WOCs.[129] Initially synthesised by Wang et al,[130] the series of $Co^{II}_3Ln^{III}$ WOC activity is highest in a pH 8 borate/HCl buffer solution with yields of O_2 between 90 - 97% and TON vales of 42 - 99. The presence of the Ln^{III} in the cubane was shown to be essential for performance enhancement, with Er^{III} and Ho^{III} analogues among leading Co^{II} containing molecular WOCs to date. The stability of the $Co^{II}_3Ln^{III}$ cores during the reaction was established with three distinct stages including spectroscopic solution tests and exclusion of nanoparticles, trace metal tests with Co^{II} chelators or ICP-MS analysis and post-catalytic structural integrity checks which encompassed HPLC analyses as well as XANES/EXAFS spectroscopy. In addition, Density Functional Theory (DFT) studies provides proof that Ln^{III} centres are active catalytic promoters with flexible ligand binding modes. Overall, this contribution has opened up 3d-4f CCs for photocatalytic applications.

Similarly, a dinuclear Fe^{III}-Ce^{IV} CC (Figure 10) with the general formula $[(Fe^{III}Ce^{IV}O(\mathbf{L34})(NO_3)_4(H_2O)](ClO_4)$ (**42-FeCe**) was reported as a catalyst for water oxidation, which was demonstrated to be a facile and reversible process.[131] The position of the equilibrium depends on the number of nitrate ligands on the Ce centre as controlled by the $MeCN/H_2O$ ratio in the solvent, which determines the $Ce^{IV/III}$ potential. A variety of characterisation techniques (single crystal X-ray diffraction, ESI-MS, XAS and TGA) were utilised to confirm the identity of **42-FeCe**. Cyclic voltammetry (CV) confirms the reversible nature of the process and represents the first examples of reversible inner-sphere electron transfer between Ce^{III} and Fe^{IV}=O CCs.

Two isostructural defected dicubane CCs with the general formula $[Mn^{II}Mn^{III}Ln^{III}_2(O_2CMe)_6$-$(H\mathbf{L35})_2(\mathbf{L36})](NO_3)\cdot H_2O$ where, Ln = Dy (**43-MnDy**) and Gd(**43-MnGd**), were reported as catalysts for water oxidation.[132] These are the first examples of mixed valent manganese (Mn^{II} and Mn^{III}) and Ln^{III} tetranuclear complexes isolated and characterised (Figure 10).

The catalytic oxidation properties of **43-MnLn** were investigated by CV in phosphate buffers at varying pH values (7 - 10). When scanned to potentials around 70 V, the CV plots for complexes **43-MnLn** show very large, irreversible oxidative waves, which correspond to catalytic water oxidation. The cyclic voltammograms of complexes **43-MnLn** in the absence of phosphate buffers or the CV of the phosphate buffer without a complex all show no catalytic current at the potential of 1.70 V.

Control potential electrolysis (CPE) experiments for **43-MnLn** complexes were recorded at a potential of 1.70 V without **43-MnLn** complexes and no catalysis was observed. In contrast, under the same conditions, but in the presence of **43-MnLn** complexes, at the applied potential the current density achieved 0.89 and 0.70 mA cm^{-2} for complexes **43-MnGd** and **43-MnDy**, respectively, revealing that both complexes are catalysts for water oxidation under these circumstances. Over an electrolysis period of 1800 s, the dissolved O_2 concentration reached 91 mM for **43-MnGd** and 76 mM for **43-MnDy**, from which we obtained estimates of TON equal to 0.36 and 0.30 for **43-MnGd** and **43-MnDy**, respectively.

3.0 Conclusions

The use of 3d-4f CCs for catalytic purposes represents a relatively unexploited extension of the traditional applications involving magnetic and luminescence studies. This review demonstrates their use in FC alkylations, Michael addition, domino ring-opening cyclization, polymerisation and redox reactions. The *in situ* dinuclear 3d-4f CC catalysts, reported by Shibasaki and co-workers, demonstrated the potential efficacy in organic transformations giving good yields, under mild reaction conditions and achieving enantioselective behaviour. Our work was the first attempt to understand the mechanisms behind 3d-4f catalysts and indeed demonstrated that with well characterised 3d-4f CCs the 3d and 4f ions could be varied; Schiff base ligands and coordination environment could be modified to enhance catalytic behaviour and alternate techniques could be used including UV-Vis, EPR and ^{1}H NMR to probe the reaction system. A feat which is not possible with pure 3d or 4f CCs. Though our work shed some light on the mechanism of 3d-4f co-operative catalysis, it also revealed limitations behind these systems including; poor solubility of high nuclearity CCs and the difficulty in developing a 3d-4f CC which is diastereoselective or enantioselective for a specific organic transformation. These results show the potential of 3d-4f CCs for catalysing organic transformations and indicate a range of ways catalysis can be evaluated. Areas for future exploration include development of heterogeneous 3d-4f CCs catalysts; investigation of other low nuclearity CC topologies; development of water soluble 3d/4f CCs and the use of 3d ions other than Ni^{II}, Cu^{II}, Zn^{II} and $Co^{II/III}$. In addition to organic transformations, the very few examples of 3d-4f CCs as oxidation catalysts have proven the combination of 3d and 4f ions can substantially improve catalytic efficacy over traditional materials and homometallic alternatives. These observations further reveal the potential catalytic applications 3d/4f CCs can be applied to.

Table 23. Reported *in situ* and well characterised 3d-4f CC pre-catalysts.

Entry	Formula / Reactants	Core	Ligand	Ref
1	$Sm(O\text{-}iPr)_3$, $Cu(OAc)_2$, H_2**L3** (1:1:1) THF	$Cu^{II}Sm^{III}$	H_2**L3**	58
2	$Sm_5O(O\text{-}iPr)_{13}$, $Cu(OAc)_2$, H_2**L3** (1:1:1), THF	$Cu^{II}Sm^{III}$	H_2**L3**	57
3	$Sm(O\text{-}iPr)_3$, $Cu(OAc)_2$, H_2**L7** (1:1:1) THF	$Cu^{II}Sm^{III}$	H_3**L7**	66
4	$Sm(OTf)_3$, $Ni(OAc)_2$, H_2**L6,** (1:1:1) THF	Ni^{II} Sm^{III}	H_2**L6**	67
5	$[Zn^{II}Yb^{III}$(**L3**)(μ_1-OAc)(μ_1-OAc)(μ_2-OAc)(H_2O)]	$Zn^{II}Yb^{III}$	H_2**L3**	70
6	$[Zn^{II}{}_2Dy^{III}{}_2$(**L3**)$_2(CO_3)_2(NO_3)_2]$	$Zn^{II}Dy^{III}$	H_2**L3**	95
7	$[Zn^{II}Y^{III}$(**L3**)$(NO_3)_2$(o-van)(MeOH)]·MeOH	$Zn^{II}Y^{III}$	H_2**L3**	95
8	$[Zn^{II}Ln^{III}$(**L3**)$(NO_3)_2$Cl(EtOH)]Ln = Dy, Gd	$Zn^{II}Ln^{III}$	H_2**L3**	95
9	$[(Fe^{III}Ce^{IV}O$(**L32**) $(NO_3)_4(H_2O)](ClO_4)$	$Fe^{III}Ce^{IV}$	**L33**	131
10	$[Zn^{II}{}_3La^{III}$(**L8**)$(NO_3)_2](NO_3)$	$Zn^{II}{}_3La^{III}$	H_6**L8**	71
11	$[Zn^{II}{}_3La^{III}$(**L8**)(OAc)$(OTf)_2]$	$Zn^{II}{}_3La^{III}$	H_6**L8**	71
12	$[Zn^{II}{}_3Ln^{III}$(**L8**)$(OAc)_3]$ Ln = La, Pr, Nd, Sm, Eu, Gd, Dy	$Zn^{II}{}_3Ln^{III}$	H_6**L8**	71
13	$[Zn^{II}{}_2Ln^{III}{}_2(\mu_3\text{-}OH)_2$(**L32**$)_4(NO_3)_4]$ Ln = Eu, Tb, Er, Yb, Nd	$Zn^{II}{}_2Ln^{III}{}_2$	H**L32**	108
14	$[Ni^{II}{}_2Dy^{III}{}_2$(**L9**$)_4(EtOH)_6](ClO_4)_2$	$Ni^{II}{}_2Dy^{III}{}_2$	H_2**L9**	82
15	$[Co^{II}{}_2Dy^{III}{}_2$(**L9**$)_4(EtOH)_6](ClO_4)_2$	$Co^{II}{}_2Dy^{III}{}_2$	H_2**L9**	82
16	$[Ni^{II}{}_2Dy^{III}{}_2$(**L9**$)_4Cl_2(MeCN)_2]$	$Ni^{II}{}_2Dy^{III}{}_2$	H_2**L9**	82
17	$[Ni^{II}{}_2Ln^{III}{}_2$(**L9**$)_4Cl_2(MeCN)_2]$ Ln = Sm, Eu, Tb, Gd, Y	$Ni^{II}{}_2Ln^{III}{}_2$	H_2**L9**	87
18	$[Ni^{II}{}_2Y^{III}{}_2$(**L10**$)_4Cl_2(MeCN)_2]$	$Ni^{II}{}_2Y^{III}$	H_2**L10**	87
19	$[Ni^{II}{}_2Y^{III}{}_2$(**L11**$)_4Cl_2(MeCN)_2]$	$Ni^{II}{}_2Y^{III}$	H_2**L11**	87
20	$[Ni^{II}{}_2Y^{III}{}_2$(**L12**$)_4Cl_2(MeCN)_2]$	$Ni^{II}{}_2Y^{III}$	H_2**L12**	87
21	$[Zn^{II}{}_2Ln^{III}{}_2$(**L9**$)_4(NO_3)_2(DMF)_2]$ Ln = Sm, Nd, Eu, Tb, Gd, Dy, Yb, Y	$Zn^{II}{}_2Ln^{III}{}_2$	H_2**L9**	92
22	$[Zn^{II}{}_2Y^{III}{}_2$(**LX**$)_4(NO_3)_2(DMF)_2]$	$Zn^{II}{}_2Y^{III}{}_2$	H_2**LX**	97
23	$[Cu^{II}{}_2Dy^{III}{}_2$(**L9**$)_4(NO_3)_2(DMF)_2]$	$Cu^{II}{}_2Dy^{III}{}_2$	H_2**L9**	97
24	$[Co^{II}{}_3Ln^{III}$(**L31**$)_4$(OAc) $(H_2O)_5]$ Ln = Ho, Er, Tm, Yb	$Co^{II}{}_3Ln^{III}$	H**L32**	129
25	$[Mn^{II}Mn^{III}Ln^{III}{}_2(O_2CMe)_6$-(H**L34**$)_2$(**L35**$)](NO_3)\cdot H_2O$ Ln = Dy, Gd	$Mn^{II}Mn^{III}Ln^{III}{}_2$	H_2**L34**	132
26	$[Zn^{II}{}_4Ln^{III}{}_2(\mu_3$ -OH$)_2$(**L32**$)_4(OAc)_6(NO_3)_2]$ Ln = Eu, Tb	$Zn^{II}{}_4Ln^{III}{}_2$	H**L32**	108
27	$[Zn^{II}{}_4Ln^{III}{}_3$(H**L31**$)_4(NO_3)_8(H_2O)_2](NO_3)_2\cdot 2H_2O$ Ln = Dy, Gd	$Zn^{II}{}_4Ln^{III}{}_3$	H$_4$**L31**	109
28	$[Mn^{IV}{}_6Ce^{IV}O_9$(**L30**$)_9(NO_3)(H_2O)_2]$	$Mn^{IV}{}_6Ce^{IV}$	H**L31**	128

4.0 Acknowledgments

We thank the EPSRC (UK) for funding (Grant No. EP/M023834/1), the University of Sussex for offering a Ph.D. position to K. G. and Drs. John Turner and David Smith, for fruitful scientific discussions.

5.0 References

1 A. Baniodeh, N. Magnani, Y. Lan, G. Buth, C. E. Anson, J. Richter, M. Affronte, J. Schnack and A. K. Powell, *npj Quantum Mater.*, 2018, **3**, 10.

2 D. Prodius, V. Mereacre, P. Singh, Y. Lan, S. Mameri, D. D. Johnson, W. Wernsdorfer, C. E. Anson and A. K. Powell, *J. Mater. Chem. C*, 2018, **6**, 2862–2872.

3 H. Nagae, R. Aoki, S. N. Akutagawa, J. Kleemann, R. Tagawa, T. Schindler, G. Choi, T. P. Spaniol, H. Tsurugi, J. Okuda and K. Mashima, *Angew. Chemie Int. Ed.*, 2018, **57**, 2492–2496.

4 P. Abbasi, K. Quinn, D. I. Alexandropoulos, M. Damjanović, W. Wernsdorfer, A. Escuer, J. Mayans, M. Pilkington and T. C. Stamatatos, *J. Am. Chem. Soc.*, 2017, **139**, 15644–15647.

5 G. Maayan, N. Gluz and G. Christou, *Nat. Catal.*, 2018, **1**, 48–54.

6 J. Wu, X.-L. Li, M. Guo, L. Zhao, Y.-Q. Zhang and J. Tang, *Chem. Commun.*, 2018, **54**, 1065–1068.

7 J. Wu, L. Zhao, L. Zhang, X.-L. Li, M. Guo, A. K. Powell and J. Tang, *Angew. Chemie Int. Ed.*, 2016, **55**, 15574–15578.

8 M. Manoli, S. Alexandrou, L. Pham, G. Lorusso, W. Wernsdorfer, M. Evangelisti, G. Christou and A. J. Tasiopoulos, *Angew. Chem. Int. Ed.*, 2016, **55**, 679–684.

9 J.-B. Peng, Q.-C. Zhang, X.-J. Kong, Y.-Z. Zheng, Y.-P. Ren, L.-S. Long, R.-B. Huang, L.-S. Zheng and Z. Zheng, *J. Am. Chem. Soc.*, 2012, **134**, 3314–3317.

10 T. D. Pasatoiu, C. Tiseanu, A. M. Madalan, B. Jurca, C. Duhayon, J. P. Sutter and M. Andruh, *Inorg. Chem.*, 2011, **50**, 5879–5889.

11 C. Yu, Z. Zhang, L. Liu, H. Li, Y. He, X. Lu, W.-K. Wong and R. A. Jones, *New J. Chem.*, 2015, **39**, 3698–3707.

12 X. Yang, Z. Li, S. Wang, S. Huang, D. Schipper and R. A. Jones, *Chem. Commun.*, 2014, **50**, 15569–15572.

13 J. Jankolovits, C. M. Andolina, J. W. Kampf, K. N. Raymond and V. L. Pecoraro, *Angew. Chem. Int. Ed.*, 2011, **50**, 9660–9664.

14 G. Karotsis, M. Evangelisti, S. Dalgarno and E. Brechin, *Angew. Chem. Int. Ed.*, 2009, **48**, 9928–9931.

15 J.-D. Leng, J.-L. Liu and M.-L. Tong, *Chem. Commun.*, 2012, **48**, 5286–5288.

16 L. Zhang, L. Zhao, P. Zhang, C. Wang, S.-W. Yuan and J. Tang, *Inorg. Chem.*, 2015, **54**, 11535–11541.

17 J. Wu, L. Zhao, M. Guo and J. Tang, *Chem. Commun.*, 2015, **51**, 17317–17320.

18 S. Chen, V. Mereacre, G. E. Kostakis, C. E. Anson and A. K. Powell, *Inorg. Chem. Front.*, 2017, **4**, 927–934.

19 D. I. Alexandropoulos, K. M. Poole, L. Cunha-Silva, J. Ahmad Sheikh, W. Wernsdorfer, G. Christou and T. C. Stamatatos, *Chem. Commun.*, 2017, **53**, 4266–4269.

20 S. Osa, T. Kido, N. Matsumoto, N. Re, A. Pochaba and J. Mrozinski, *J. Am. Chem. Soc.*, 2004, **126**, 420–421.

21 A. M. Ako, V. Mereacre, R. Clerac, W. Wernsdorfer, I. J. Hewitt, C. E. Anson, A. K. Powell, R. Clérac, W. Wernsdorfer, I. J. Hewitt, C. E. Anson and A. K. Powell, *Chem. Commun.*, 2009, **5**, 544–546.

22 K. C. Mondal, A. Sundt, Y. Lan, G. E. Kostakis, O. Waldmann, L. Ungur, L. F. Chibotaru, C. E. Anson and A. K. Powell, *Angew. Chem. Int. Ed.*, 2012, **51**, 7550–7554.

23 F. S. Guo, B. M. Day, Y. C. Chen, M. L. Tong, A. Mansikkamäki and R. A. Layfield, *Angew. Chemie - Int. Ed.*, 2017, **56**, 11445–11449.

24 C. A. P. Goodwin, F. Ortu, D. Reta, N. F. Chilton and D. P. Mills, *Nature*, 2017, **548**, 439–442.

25 M. Andruh, *Dalton Trans.*, 2015, **44**, 16633–16653.
26 S. Chen, V. Mereacre, Z. Zhao, W. Zhang, M. Zhang and Z. He, *Dalton Trans.*, , DOI:10.1039/C8DT01289J.
27 J. Goura, R. Guillaume, E. Rivière and V. Chandrasekhar, *Inorg. Chem.*, 2014, **53**, 7815–7823.
28 V. Chandrasekhar, A. Dey, S. Das, M. Rouzières and R. Clérac, *Inorg. Chem.*, 2013, **52**, 2588–2598.
29 E. Moreno Pineda, N. F. Chilton, F. Tuna, R. E. P. Winpenny and E. J. L. McInnes, *Inorg. Chem.*, 2015, **54**, 5930–5941.
30 T. N. Hooper, J. Schnack, S. Piligkos, M. Evangelisti and E. K. Brechin, *Angew. Chem. Int. Ed.*, 2012, **51**, 4633–4636.
31 E. Loukopoulos, K. Griffiths, G. R. Akien, N. Kourkoumelis, A. Abdul-Sada and G. E. Kostakis, *Inorganics*, 2015, **3**, 448–466.
32 S. Rast, A. Borel, L. Helm, E. Belorizky, P. H. Fries and A. E. Merbach, *J. Am. Chem. Soc.*, 2001, **123**, 2637–2644.
33 A. Szyczewski, S. Lis, Z. Kruczyński, J. Pietrzak, S. But and M. Elbanowski, *Acta Phys. Pol. A*, 1996, **90**, 345–351.
34 G. K. Veits and J. Read de Alaniz, *Tetrahedron*, 2012, **68**, 2015–2026.
35 A. I. Nguyen, J. Wang, D. S. Levine, M. S. Ziegler and T. D. Tilley, *Chem. Sci.*, 2017, **8**, 4274–4284.
36 E. B. Clatworthy, X. Li, A. F. Masters and T. Maschmeyer, *Chem. Commun.*, 2016, **52**, 14412–14415.
37 E. F. DiMauro and M. C. Kozlowski, *Org. Lett.*, 2001, **3**, 1641–1644.
38 V. Annamalai, E. F. DiMauro, P. J. Carroll and M. C. Kozlowski, *J. Org. Chem.*, 2003, **68**, 1973–1981.
39 E. F. DiMauro and M. C. Kozlowski, *Organometallics*, 2002, **21**, 1454–1461.
40 M. Yang, C. Zhu, F. Yuan, Y. Huang and Y. Pan, *Org. Lett.*, 2005, **7**, 1927–1930.
41 J. Sun, F. Yuan, M. Yang, Y. Pan and C. Zhu, *Tetrahedron Lett.*, 2009, **50**, 548–551.
42 J. Park and S. Hong, *Chem. Soc. Rev.*, 2012, **41**, 6931–6943.
43 S. Matsunaga and M. Shibasaki, *Chem. Commun.*, 2014, **50**, 1044–1057.
44 N. E. Shepherd, H. Tanabe, Y. Xu, S. Matsunaga and M. Shibasaki, *J. Am. Chem. Soc.*, 2010, **132**, 3666–3667.
45 Z. Chen, K. Yakura, S. Matsunaga and M. Shibasaki, *Org. Lett.*, 2008, **10**, 3239–3242.
46 Z. Chen, H. Morimoto, S. Matsunaga and M. Shibasaki, *J. Am. Chem. Soc.*, 2008, **130**, 2170–2171.
47 Y. Kato, Z. Chen, S. Matsunaga and M. Shibasaki, *Synlett*, 2009, **2009**, 1635–1638.
48 Y. Xu, S. Matsunaga and M. Shibasaki, *Org. Lett.*, 2010, **12**, 3246–3249.
49 M. S. irooki Tanabe, Yingjie Xu, Bo Sun, Shigeki Matsunaga, *Heterocycles*, 2012, **1**, 611–622.
50 S. Mouri, Z. Chen, H. Mitsunuma, M. Furutachi, S. Matsunaga and M. Shibasaki, *J. Am. Chem. Soc.*, 2010, **132**, 1255–1257.
51 P. Gopinath, T. Watanabe and M. Shibasaki, *Org. Lett.*, 2012, **14**, 1358–1361.
52 S. Mouri, Z. Chen, S. Matsunaga and M. Shibasaki, *Chem. Commun.*, 2009, 5138–5140.
53 S. Kato, M. Kanai and S. Matsunaga, *Chem. – An Asian J.*, 2013, **8**, 1768–1771.
54 M. Furutachi, Z. Chen, S. Matsunaga and M. Shibasaki, *Molecules*, 2010, **15**, 532–544.
55 Z. Chen, M. Furutachi, Y. Kato, S. Matsunaga and M. Shibasaki, *Angew. Chemie Int. Ed.*, 2009, **48**, 2218–2220.
56 Y. Kato, M. Furutachi, Z. Chen, H. Mitsunuma, S. Matsunaga and M. Shibasaki, *J. Am. Chem. Soc.*, 2009, **131**, 9168–9169.
57 S. Handa, V. Gnanadesikan, S. Matsunaga and M. Shibasaki, *J. Am. Chem. Soc.*, 2010,

132, 4925–4934.
58 S. Handa, V. Gnanadesikan, S. Matsunaga and M. Shibasaki, *J. Am. Chem. Soc.*, 2007, **129**, 4900–4901.
59 S. Handa, K. Nagawa, Y. Sohtome, S. Matsunaga and M. Shibasaki, *Angew. Chem. Int. Ed.*, 2008, **47**, 3230–3233.
60 Y. Sohtome, Y. Kato, S. Handa, N. Aoyama, K. Nagawa, S. Matsunaga and M. Shibasaki, *Org. Lett.*, 2008, **10**, 2231–2234.
61 L. Liu, Z. Zhang, W. Feng, C. Yu, X. Lü, W.-K. Wong and R. A. Jones, *Inorg. Chem. Commun.*, 2014, **49**, 124–126.
62 Y. Zhang, W. Feng, H. Liu, Z. Zhang, X. Lü, J. Song, D. Fan, W. K. Wong and R. A. Jones, *Inorg. Chem. Commun.*, 2012, **24**, 148–152.
63 W. X. Feng, Y. N. Hui, G. X. Shi, D. Zou, X. Q. Lü, J. R. Song, D. Di Fan, W. K. Wong and R. A. Jones, *Inorg. Chem. Commun.*, 2012, **20**, 33–36.
64 Y.-M. Tian, H.-F. Li, B.-L. Han, Q. Zhang and W.-B. Sun, *Acta Crystallogr. Sect. E Struct. Reports Online*, 2012, **68**, m1500–m1501.
65 P. Zhang, L. Zhang, S.-Y. Lin and J. Tang, *Inorg. Chem.*, 2013, **52**, 6595–6602.
66 Y. Li, P. Deng, Y. Zeng, Y. Xiong and H. Zhou, *Org. Lett.*, 2016, **18**, 1578–1581.
67 M. Furutachi, S. Mouri, S. Matsunaga and M. Shibasaki, *Chem. – An Asian J.*, 2010, **5**, 2351–2354.
68 K. C. Mondal, G. E. Kostakis, Y. Lan, W. Wernsdorfer, C. E. Anson and A. K. Powell, *Inorg. Chem.*, 2011, **50**, 11604–11611.
69 K. Griffiths, V. N. Dokorou, J. Spencer, A. Abdul-Sada, A. Vargas and G. E. Kostakis, *CrystEngComm*, 2016, **18**, 704–713.
70 Q. Shi, X. Yang, X. Zhang, X. Li, J. Yang and X. Lü, *Inorg. Chem. Commun.*, 2016, **73**, 4–6.
71 H. Nagae, R. Aoki, S. N. Akutagawa, J. Kleemann, R. Tagawa, T. Schindler, G. Choi, T. P. Spaniol, H. Tsurugi, J. Okuda and K. Mashima, *Angew. Chemie - Int. Ed.*, 2018, **57**, 2492–2496.
72 D. J. Darensbourg and A. D. Yeung, *Polym. Chem.*, 2014, **5**, 3949–3962.
73 D. R. Moore, M. Cheng, E. B. Lobkovsky and G. W. Coates, *J. Am. Chem. Soc.*, 2003, **125**, 11911–11924.
74 S. M. Ahmed, A. Poater, M. I. Childers, P. C. B. Widger, A. M. LaPointe, E. B. Lobkovsky, G. W. Coates and L. Cavallo, *J. Am. Chem. Soc.*, 2013, **135**, 18901–18911.
75 D. J. Darensbourg, M. W. Holtcamp, G. E. Struck, M. S. Zimmer, S. A. Niezgoda, P. Rainey, J. B. Robertson, J. D. Draper and J. H. Reibenspies, *J. Am. Chem. Soc.*, 1999, **121**, 107–116.
76 E. Hosseini Nejad, A. Paoniasari, C. E. Koning and R. Duchateau, *Polym. Chem.*, 2012, **3**, 1308–1313.
77 X.-B. Lu and D. J. Darensbourg, *Chem. Soc. Rev.*, 2012, **41**, 1462–1484.
78 K. B. Hansen, J. L. Leighton and E. N. Jacobsen, *J. Am. Chem. Soc.*, 1996, **118**, 10924–10925.
79 D. Liu, X. Zhang, L. Zhu, J. Wu and X. Lu, *Catal. Sci. Technol.*, 2015, **5**, 562–571.
80 S. I. Vagin, R. Reichardt, S. Klaus and B. Rieger, *J. Am. Chem. Soc.*, 2010, **132**, 14367–14369.
81 M. R. Kember, F. Jutz, A. Buchard, A. J. P. White and C. K. Williams, *Chem. Sci.*, 2012, **3**, 1245–1255.
82 K. Griffiths, C. W. D. Gallop, A. Abdul-Sada, A. Vargas, O. Navarro and G. E. Kostakis, *Chem. Eur. J.*, 2015, **21**, 6358–6361.
83 S.-W. Li and R. A. Batey, *Chem. Commun.*, 2007, 3759–3761.
84 R. F. A. Gomes, N. R. Esteves, J. A. S. Coelho and C. A. M. Afonso, *J. Org. Chem.*,

2018, acs.joc.7b02931.
85 R. F. A. Gomes, J. A. S. Coelho and C. A. M. Afonso, *Chem. - A Eur. J.*, , DOI:10.1002/chem.201705851.
86 M. Nardi, P. Costanzo, A. De Nino, M. L. Di Gioia, F. Olivito, G. Sindona and A. Procopio, *Green Chem.*, 2017, **19**, 5403–5411.
87 K. Griffiths, P. Kumar, J. D. Mattock, A. Abdul-Sada, M. B. Pitak, S. J. Coles, O. Navarro, A. Vargas and G. E. Kostakis, *Inorg. Chem.*, 2016, **55**, 6988–6994.
88 G. Zhang, Y. Wei, L. Guo, X. Zhu, S. Wang, S. Zhou and X. Mu, *Chem. - A Eur. J.*, 2015, **21**, 2519–2526.
89 R. F. A. Gomes, N. R. Esteves, J. A. S. Coelho and C. A. M. Afonso, *J. Org. Chem.*, , DOI:10.1021/acs.joc.7b02931.
90 D. Chen, L. Yu and P. G. Wang, *Tetrahedron Lett.*, 1996, **37**, 4467–4470.
91 Y. H. Hui, Y. C. Chen, H. W. Gong and Z. F. Xie, *Chinese Chem. Lett.*, 2014, **25**, 163–165.
92 K. Griffiths, P. Kumar, G. R. Akien, N. F. Chilton, A. Abdul-Sada, G. J. Tizzard, S. J. Coles and G. E. Kostakis, *Chem. Commun.*, 2016, **52**, 7866–7869.
93 P. Kumar, S. Lymperopoulou, K. Griffiths, S. Sampani and G. Kostakis, *Catalysts*, 2016, **6**, 140.
94 A. L. Gemal and J. L. Luche, *J. Am. Chem. Soc.*, 1981, **103**, 5454–5459.
95 S. I. Sampani, S. Aubert, M. Cattoen, K. Griffiths, A. Abdul-Sada, G. Akien, G. J. Tizzard, S. Coles, S. Arseniyadis and G. E. Kostakis, *Dalton Trans.*, 2018, **47**, 4486–4493.
96 P. Kumar, K. Griffiths, S. Lymperopoulou, G. E. Kostakis and G. E. Kostakis, *RSC Adv.*, 2016, **6**, 79180–79184.
97 K. Griffiths, A. C. Tsipis, P. Kumar, O. P. E. Townrow, A. Abdul-Sada, G. R. Akien, A. Baldansuren, A. C. Spivey and G. E. Kostakis, *Inorg. Chem.*, 2017, **56**, 9563–9573.
98 P. Howlader, P. Das, E. Zangrando and P. S. Mukherjee, *J. Am. Chem. Soc.*, 2016, **138**, 1668–1676.
99 H. J. Al-Najjar, A. Barakat, A. M. Al-Majid, Y. N. Mabkhot, M. Weber, H. A. Ghabbour and H.-K. Fun, *Molecules*, 2014, **19**, 1150–1162.
100 F. Seeliger, S. T. A. Berger, G. Y. Remennikov, K. Polborn and H. Mayr, *J. Org. Chem.*, 2007, **72**, 9170–9180.
101 M. Rombola, C. S. Sumaria, T. D. Montgomery and V. H. Rawal, *J. Am. Chem. Soc.*, 2017, **139**, 5297–5300.
102 N. R. Penthala, A. Ketkar, K. R. Sekhar, M. L. Freeman, R. L. Eoff, R. Balusu and P. A. Crooks, *Bioorganic Med. Chem.*, 2015, **23**, 7226–7233.
103 T. Sakakura and K. Kohno, *Chem. Commun.*, 2009, 1312–1330.
104 J. Hu, J. Ma, Q. Zhu, Q. Qian, H. Han, Q. Mei and B. Han, *Green Chem.*, 2016, **18**, 382–385.
105 J. Qin, P. Wang, Q. Li, Y. Zhang, D. Yuan and Y. Yao, *Chem. Commun.*, 2014, **50**, 10952–10955.
106 J. Dong, P. Cui, P.-F. Shi, P. Cheng and B. Zhao, *J. Am. Chem. Soc.*, 2015, **137**, 15988–15991.
107 J. A. Garden, P. K. Saini and C. K. Williams, *J. Am. Chem. Soc.*, 2015, **137**, 15078–15081.
108 J. Qin, B. Xu, Y. Zhang, D. Yuan and Y. Yao, *Green Chem.*, 2016, **18**, 4270–4275.
109 L. Wang, C. Xu, Q. Han, X. Tang, P. Zhou, R. Zhang, G. Gao, B. Xu, W. Qin and W. Liu, *Chem. Commun.*, 2018, **54**, 2212–2215.
110 R. Zhang, L. Wang, C. Xu, H. Yang, W. Chen, G. Gao and W. Liu, *Dalton Trans.*, 2018, **47**, 7159–7165.

111 M. V. Escárcega-Bobadilla, M. Martínez Belmonte, E. Martin, E. C. Escudero-Adán and A. W. Kleij, *Chem. - A Eur. J.*, 2013, **19**, 2641–2648.

112 R. M. Haak, A. Decortes, E. C. Escudero-Adán, M. M. Belmonte, E. Martin, J. Benet-Buchholz and A. W. Kleij, *Inorg. Chem.*, 2011, **50**, 7934–7936.

113 R. Ma, L.-N. He and Y.-B. Zhou, *Green Chem.*, 2016, **18**, 226–231.

114 M. Chihiro, T. Tomoya, O. Kanae and E. Tadashi, *Angew. Chemie Int. Ed.*, 2014, **54**, 134–138.

115 C. J. Whiteoak, N. Kielland, V. Laserna, E. C. Escudero-Adán, E. Martin and A. W. Kleij, *J. Am. Chem. Soc.*, 2013, **135**, 1228–1231.

116 M. D. Kärkäs and B. Åkermark, *Dalton Trans.*, 2016, **45**, 14421–14461.

117 N. S. McCool, D. M. Robinson, J. E. Sheats and G. C. Dismukes, *J. Am. Chem. Soc.*, 2011, **133**, 11446–11449.

118 T. G. Carrell, S. Cohen and G. C. Dismukes, *J. Mol. Catal. A Chem.*, 2002, **187**, 3–15.

119 P. Kurz, G. Berggren, M. F. Anderlund and S. Styring, *Dalton Trans.*, 2007, **38**, 4258.

120 J. Limburg, J. S. Vrettos, L. M. Liable-Sands, A. L. Rheingold, R. H. Crabtree and G. W. Brudvig, *Science (80-.).*, 1999, **283**, 1524–1527.

121 A. K. Poulsen, A. Rompel and C. J. McKenzie, *Angew. Chemie Int. Ed.*, 2005, **44**, 6916–6920.

122 M. M. Najafpour, A. N. Moghaddam, D. J. Sedigh and M. Holynska, *Catal. Sci. Technol.*, 2014, **4**, 30–33.

123 Y. Liu, R. Xiang, X. Du, Y. Ding and B. Ma, *Chem. Commun.*, 2014, **50**, 12779–12782.

124 A. R. Parent, T. Nakazono, S. Lin, S. Utsunomiya and K. Sakai, *Dalton Trans.*, 2014, **43**, 12501–12513.

125 M. Okamura, M. Kondo, R. Kuga, Y. Kurashige, T. Yanai, S. Hayami, V. K. K. Praneeth, M. Yoshida, K. Yoneda, S. Kawata and S. Masaoka, *Nature*, 2016, **530**, 465–468.

126 B. L. Lee, M. D. Kärkäs, E. V. Johnston, A. K. Inge, L. H. Tran, Y. Xu, Ö. Hansson, X. Zou and B. Akermark, *Eur. J. Inorg. Chem.*, 2010, 5462–5470.

127 S. Nayak, H. P. Nayek, S. Dehnen, A. K. Powell and J. Reedijk, *Dalton Trans.*, 2011, **40**, 2699–2702.

128 G. Maayan and G. Christou, *Inorg. Chem.*, 2011, **50**, 7015–7021.

129 F. Evangelisti, R. More, F. Hodel, S. Luber and G. R. Patzke, *J. Am. Chem. Soc.*, 2015, **137**, 11076–11084.

130 P. Wang, S. Shannigrahi, N. L. Yakovlev and T. S. A. Hor, *Inorg. Chem.*, 2012, **51**, 12059–12061.

131 A. Draksharapu, W. Rasheed, J. E. M. N. Klein and L. Que, *Angew. Chemie Int. Ed.*, 2017, **56**, 9091–9095.

132 T.-X. Lan, W.-S. Gao, C.-N. Chen, H.-S. Wang, M. Wang and Y. Fan, *New J. Chem.*, 2018, **42**, 5798–5805.